UPPSALA
UNIVERSITET

Digital Comprehensive Summaries of Uppsala Dissertations from the Faculty of Science and Technology 775

Multipoles in Correlated Electron Materials

FRANCESCO CRICCHIO

ACTA
UNIVERSITATIS
UPSALIENSIS
UPPSALA
2010

ISSN 1651-6214
ISBN 978-91-554-7917-6
urn:nbn:se:uu:diva-132068

Dissertation presented at Uppsala University to be publicly examined in Siegbahnsalen, Ångströmlaboratoriet, Lägerhyddsvägen 1, Uppsala, Friday, November 26, 2010 at 13:15 for the degree of Doctor of Philosophy. The examination will be conducted in English.

Abstract
Cricchio, F. 2010. Multipoles in Correlated Electron Materials. Acta Universitatis Upsaliensis. *Digital Comprehensive Summaries of Uppsala Dissertations from the Faculty of Science and Technology* 775. 84 pp. Uppsala. ISBN 978-91-554-7917-6.

Electronic structure calculations constitute a valuable tool to predict the properties of materials. In this study we propose an efficient scheme to study correlated electron systems with essentially only one free parameter, the screening length of the Coulomb potential. A general reformulation of the exchange energy of the correlated electron shell is combined with this method in order to analyze the calculations. The results are interpreted in terms of different polarization channels, due to different multipoles. The method is applied to various actinide compounds, in order to increase the understanding of the complicate behaviour of 5*f* electrons in these systems. We studied the non-magnetic phase of δ-Pu, where the spin polarization is taken over by a spin-orbit-like term that does not break the time reversal symmetry. We also find that a non-trivial high multipole of the magnetization density, the triakontadipole, constitutes the ordering parameter in the mysterious hidden order phase of the heavy-fermion superconductor URu_2Si_2. This type of multipolar ordering is also found to play an essential role in the hexagonal-based superconductors UPd_2Al_3, UNi_2Al_3 and UPt_3 and in the dioxide insulators UO_2, NpO_2 and PuO_2. The triakontadipole moments are also present in all magnetic actinides we considered, except for Cm. These results led us to formulate a new set of rules for the ground state of a system, that are valid in presence of strong spin-orbit coupling interaction instead of those of Hund; the Katt's rules. Finally, we applied our method to a new class of high-T_c superconductors, the Fe-pnictides, where the Fe 3*d* electrons are moderately correlated. In these materials we obtain the stabilization of a low spin moment solution, in agreement with experiment, over a large moment solution, due to the gain in exchange energy in the formation of large multipoles of the spin magnetization density.

Keywords: correlated electrons, magnetic ordering, multipoles, actinides, hidden order, high temperature superconductors, Fe pnictides, electronic structure calculations

Francesco Cricchio, Department of Physics and Astronomy, Materials Theory, Box 516, Uppsala University, SE-751 20 Uppsala, Sweden.

ISSN 1651-6214
ISBN 978-91-554-7917-6
urn:nbn:se:uu:diva-132068 (http://urn.kb.se/resolve?urn=urn:nbn:se:uu:diva-132068)

To my parents and to my brother

“I don’t want to achieve immortality through my work...I want to achieve it through not dying."

Woody Allen

List of Papers

This thesis is based on the following papers, which are referred to in the text by their Roman numerals.

I **Low spin moment due to hidden multipole order from spin-orbital ordering in LaFeAsO.** F. Cricchio, O. Grånäs and L. Nordström, Phys. Rev. B (RC) **81**, 140403 (2010).

II **Multipole decomposition of LDA+U energy and its application to actinide compounds.** F. Bultmark, F. Cricchio, O. Grånäs and L. Nordström, Phys. Rev. B **80**, 035121 (2009).

III **Itinerant magnetic multipole moments of rank five as the hidden order in URu_2Si_2.** F. Cricchio, F. Bultmark, O. Grånäs and L. Nordström, Phys. Rev. Lett. **103**, 107202 (2009).

IV **Exchange energy dominated by large orbital spin-currents in δ-Pu.** F. Cricchio, F. Bultmark and L. Nordström , Phys. Rev. B (RC) **78** 100404 (2008).

V **The role of magnetic triakontadipoles in uranium-based superconductor materials.** F. Cricchio, O. Grånäs and L. Nordström , preprint.

VI **Multipolar and orbital ordering in ferro-pnictides.** F. Cricchio, O. Grånäs and L. Nordström, preprint.

VII **Multipolar magnetic ordering in actinide dioxides from first-principles calculations.** F. Cricchio, O. Grånäs and L. Nordström, preprint.

VIII **Polarization of an open shell in the presence of spin-orbit coupling.** F. Cricchio, O. Grånäs and L. Nordström, preprint.

IX **Analysis of dynamical exchange and correlation in terms of coupled multipoles.** O. Grånäs, F. Cricchio, F. Bultmark, I. Di Marco and L. Nordström, preprint.

Related Work

I **Distorted space and multipoles in electronic structure calculations.** F. Bultmark, Ph.d Thesis, Uppsala University (2009).

II **Intra atomic exchange and magnetism in heavy elements.** O. Grånäs, Licentiate Thesis, Uppsala University (2009).

III **High-pressure melting of lead**. F. Cricchio, A. Belonoshko, L. Burakovsky, D.L. Preston and R. Ahuja, Phys. Rev. B (RC) **73**, 140103 (2006).

Contents

1 Introduction 11
2 Density Functional Theory 15
2.1 The Many Body Problem 15
2.2 The Hohenberg-Kohn Formulation of DFT 17
2.3 The Self-Consistent Kohn-Sham Equations 18
2.4 Approximations for the Exchange-Correlation Potential 20
3 The APW+lo Basis Set 21
3.1 APW Method 21
3.2 Introduction of Local Orbitals 23
3.3 Treatment of Core Electrons 23
4 Intra-atomic Non-collinear Magnetism 25
4.1 Spin-dependent DFT 25
4.2 Spin-spirals 26
4.3 Spin-orbit Interaction 28
4.4 Second-variational Approach to Magnetism 30
4.5 Fixed Spin Moment Calculations 32
5 A General Form of LDA+U Method 33
5.1 Slater Integrals Screened by Yukawa Potential 33
5.2 Calculation of LDA+U Potential 35
5.3 Double-Counting Corrections 35
5.4 Multipole Representation of LDA+U Energy 38
5.5 The Coupling of Indices - Irreducible Spherical Tensor 42
5.6 Physical Interpretation of Tensor Moments 44
5.7 Polarization Channels 44
6 Analysis of Results and Discussion 49
6.1 Enhancement of Orbital Spin Currents in δ-Pu 49
6.2 Triakontadipoles in Uranium Magnetic Compounds 53
6.3 Triakontadipoles Moments as the Hidden Order in URu_2Si_2 . . . 53
6.4 Triakontadipoles in Hexagonal Actinide Superconductors 57
6.5 Multipolar Magnetic Ordering in Actinide Dioxides 58
6.6 Time Reversal Symmetry Breaking in Itinerant Systems 58
6.6.1 Hund's Rules 58
6.6.2 Katt's Rules 59
6.7 Low Spin Moment due to Hidden Multipole Order in ferro-pnictides 63
7 Conclusions 69

8 Sammanfattning på svenska 73
Bibliography 79

1. Introduction

Electrons and nuclei are the fundamental particles that determine the nature of the matter of our world. The fundamental basis for understanding materials and phenomena ultimately rests upon understanding electronic structure. In 1929 Paul Dirac wrote [1] that with the discovery of quantum mechanics: "The underlying laws necessary for the mathematical theory of a large part of physics and the whole of chemistry are thus completely known, and the difficulty is only that exact applications of these laws lead to equations which are too complicated to be soluble". Today it exists a very efficient method to deal with these equations in solids by use of modern computers; density functional theory (DFT) [2]. Within DFT approach the properties of compounds can be determined by mapping the many-electron problem to one-electron effective problem expressed in terms of functionals of the electron density. Although ordinary DFT has proven to be very accurate for a wide range of materials, it often fails to capture the fundamental physics of systems with open d and f shells where the electrons are localized and the Coulomb repulsion is large. In this case the electrons can no longer be treated as independent and the movement of one electron strongly depends on the position of the others; the electrons are called strongly correlated.

In material science, magnetism remains one of the essential areas of study, although the properties of magnetic compounds have been used for applications already for many years. The ongoing research remains extensive and intense, as still to date revolutionary new effects related to magnetic interactions are revealed. The competing couplings between lattice, charge, spin and orbital degrees of freedom in crystals are related in a complex equilibrium that in special cases results in fascinating and novel phenomena. A class of compounds that shows a rich variety of exotic magnetic properties are the actinides [3]. There are variations from itinerant magnetic systems to systems showing characteristics of localized magnetism. In the border between these extremes one have the so-called heavy fermions, which show many anomalous properties, one of which is the coexistence of superconductivity and magnetism [4]. One aspect that makes the magnetism of the actinides unique is the co-existence of strong spin-orbit coupling (SOC) and strong exchange interactions among the $5f$ electrons, which are the ones responsible for the magnetism. From a theoretical point of view, a standard DFT approach, either in the local density approximation

(LDA) or generalized gradient approximation (GGA), describes quite well the equilibrium properties of metallic systems. However, in actinides these functionals underestimate the orbital moments which are induced by the strong SOC interaction [5, 6, 7]. This deficiency can be remedied by allowing for the so-called orbital polarization [7], responsible for Hund's second rule in atomic physics, either through adding an appropriate orbital depending term to the Hamiltonian or by adopting the so-called LDA+U approach [8, 9, 10]. In the latter method a screened Hartree-Fock (HF) interaction is included among the correlated electrons only.
Magnetic ordering is relatively abundant among actinide systems due to the strong exchange interactions, but generally the spin moments are strongly reduced compared to a fully spin polarized value. This work will focus on the role of the local screened exchange interactions; it will aim to convincingly argue that these interactions are responsible for the reduced spin polarizations as well as for a large orbital moment in many actinide compounds. One of the most controversial discussion in the field of actinides concerns the absence of magnetic moments in the anomalous high-pressure δ-phase of Pu [3]. This study will provide an explanation of the vanishing of magnetism in this material in terms of enhancement of the SOC channel in the exchange energy (see papers IV and IX). This work will also focus on the mysterious hidden order phase of the heavy-fermion superconductor URu_2Si_2 [11]. In our study we find that a high multipole of the magnetization density, the triakontadipole, is the main order parameter in URu_2Si_2 (see paper III). The triakontadipole ordering is also determined to play an essential role in other actinide superconductors, UPd_2Al_3, UNi_2Al_3 and UPt_3 (see paper V) and in the actinide dioxide insulators, UO_2, NpO_2 and PuO_2 (see paper VII). These results lead us to formulate a new set of rules, the Katt's rules, that are valid for the ground state of itinerant systems with strong SOC interaction, instead of Hund's rules (see paper VIII).
In order attack these problems we developed an efficient scheme to treat electron correlation with LDA+U method and only one free parameter (see paper II). This is accomplished by using Slater parameters screened by a Yukawa potential together with an interpolating optimal double-counting term [12]. This last degree of freedom can be chosen to be, for instance, the lowest Slater integral U, which is used as a varying parameter. At the same time we introduced an analysis method for the resulting ground state. This analysis is based on an exact multipole decomposition of the density matrix as well as of the HF exchange energy.

Another class of compounds that created a large interest in the scientific community are the high critical temperature (T_C) cuprate superconductors because of the ambiguous coexistence and interplay between superconductivity and magnetism. Recently, the discovery of a new class of high-T_C superconductors, the ferro-pnictides [13], has raised the hope of

understanding the elusive mechanism of the high-T_C superconductivity of the cuprates [14]. Indeed there are many similarities between the two classes of compounds; the fact that the parent compound is antiferromagnetic (AF), the key role played by a transition-metal layer, the fact that the AF order quickly disappears with doping and then is overtaken by a strong superconducting state. However, some differences were also discovered. While the main electrons in the cuprates are correlated and close to an insulating state, in the ferro-pnictides they seems to be moderately correlated and metallic [15, 16]. With the increasing number of theoretical studies, it has been clarified that DFT shows some difficulties in treating the iron pnictide compounds. The calculations systematically predict unusually bad Fe-As bonding distances and largely overestimate the ordered AF spin moment [17, 18]. This work will show that, by including on-site correlation effects in the calculation of ferro-pnictides electronic structure, a low-spin moment solution in agreement with experiment [19] is stabilized due to polarization of higher multipole moments of the spin density (see papers I and VI). It is also found that the calculated equilibrium distance between the Fe plane and the As planes is in good agreement with the measured value [19]. Finally, we will also make a comparison with the LDA+U solution for an undoped cuprate, $CaCuO_2$, which reveals a striking similarity in the role played by magnetic multipoles.

The thesis is organized as follows: chapter 2 reviews the density functional theory approach to treat many-electrons systems, chapter 3 describes the power of APW+lo basis set to solve the Kohn-Sham equation, chapter 4 summarizes the treatment of non-collinear magnetism, and, finally, chapter 5 deals with LDA+U method and its multipole expansion. The applications of these methods to different actinide and pnictide systems are discussed in chapter 6, for example, by observing several clear trends regarding the favoured polarizations of exchange energy channels. Finally, we draw our conclusions in chapter 7.

2. Density Functional Theory

2.1 The Many Body Problem

The Hamiltonian for the system of electrons and nuclei in a solid can be written as

$$\begin{aligned}\mathscr{H} = &-\frac{1}{2}\sum_{i=1}\nabla_i^2 - \sum_{i,I}\frac{Z_I}{|\boldsymbol{r}_i - \boldsymbol{R}_I|} + \frac{1}{2}\sum_{i\neq j}\frac{1}{|\boldsymbol{r}_i - \boldsymbol{r}_j|} \\ &-\frac{1}{2}\sum_{I}\frac{\nabla_I^2}{M_I} + \frac{1}{2}\sum_{I\neq J}\frac{Z_I Z_J}{|\boldsymbol{R}_I - \boldsymbol{R}_J|}\ ,\end{aligned} \tag{2.1}$$

where $\boldsymbol{r}_i$ are the positions of the electrons, $\boldsymbol{R}_I$ and Z_I are, respectively, the nuclei positions and the atomic number, M_I is the nucleus mass. Here, and in what follows, atomic units are used.
The Hamiltonian in Eq. (2.1) can be written more schematically as

$$\mathscr{H} = \mathscr{T}_{\mathrm{e}} + \mathscr{V}_{\mathrm{eI}} + \mathscr{V}_{\mathrm{ee}} + \mathscr{T}_{\mathrm{I}} + \mathscr{V}_{\mathrm{II}}\ , \tag{2.2}$$

where $\mathscr{T}_{\mathrm{e}}$ and $\mathscr{T}_{\mathrm{I}}$ are, respectively, the electronic and the nuclei kinetic energy, while the terms $\mathscr{V}_{\mathrm{ee}}$, $\mathscr{V}_{\mathrm{II}}$, $\mathscr{V}_{\mathrm{eI}}$ correspond to Coulomb interaction between, respectively, electrons, nuclei, electrons and nuclei. Because of the large difference in mass between electrons and nuclei, the electrons respond essentially instantaneously to the motion of the nuclei. Therefore the many-body problem is reduced to the solution of the electronic part in some frozen configuration of the nuclei (or of atomic cores). This is the so-called Born-Oppenheimer approximation. Even with this simplifications, the many-body problem remains formidable. Density functional theory (DFT) is a valuable tool to calculate an approximate solution to the ground-state energy of N interacting electrons in the external potential arising from the nuclei. Once the electrons have been relaxed to their instantaneous ground-state, the interaction between the nuclei $\mathscr{V}_{II}$ (or between the atomic cores) is treated classically by means of Ewald method [20]. For a given nuclei positions, the fundamental Hamiltonian for the theory of electronic structure of matter is

$$\mathscr{H} = \mathscr{T}_{\mathrm{e}} + \mathscr{V}_{\mathrm{eI}} + \mathscr{V}_{\mathrm{ee}}\ . \tag{2.3}$$

The electronic structure is determined by the solutions of the Schrödinger equation of N electrons

$$\mathscr{H}\Psi = \left\{ -\frac{1}{2}\sum_i \nabla_i^2 + \sum_i v(\boldsymbol{r}_i) + \frac{1}{2}\sum_{i\neq j}\frac{1}{|\boldsymbol{r}_i - \boldsymbol{r}_j|} \right\}\Psi = E\Psi \ , \tag{2.4}$$

where $\Psi = \Psi(x_1, x_2, \ldots x_N)$ is the N-electron wavefunction, with x's indicating both spatial and spin coordinates and where $v(\boldsymbol{r}_i)$ refers to the potential experienced by the electron i due to the nuclei,

$$v(\boldsymbol{r}_i) = \sum_I \frac{Z_I}{|\boldsymbol{r}_i - \boldsymbol{R}_I|} \ . \tag{2.5}$$

In the Born-Oppenheimer approximation, all the physical properties of the electrons depend parametrically on the nuclei positions $\boldsymbol{R}_I$. The electron density $n(\boldsymbol{r})$ and the total energy E can be written as

$$n(\boldsymbol{r}) = n(\boldsymbol{r}; \boldsymbol{R}_1, \ldots \boldsymbol{R}_M), \qquad E = E(\boldsymbol{R}_1, \ldots \boldsymbol{R}_M) \ , \tag{2.6}$$

where M indicates the number of nuclei.
As W. Kohn clearly emphasized in his Nobel lecture [2], the solution of problem (2.4) is not feasible by traditional wave-function methods in case of condensed matter systems, where $N \sim 10^{22}/\mathrm{cm}^3$ electrons. Let us consider a general molecule consisting of M atoms with a total of N interacting electrons, where $M \gg 10$. Ideally we would like to find the ground-state energy E by Rayleigh-Ritz variational principe,

$$E = \min_{\Psi} \left\langle \Psi | \mathscr{H} | \Psi \right\rangle \ , \qquad \int |\Psi(x_1, x_2 \ldots x_N)|^2 dx_1 dx_2 \ldots dx_N = 1 \ . \tag{2.7}$$

We should do this by including K parameters $p_1, p_2 \ldots p_K$ in a trial wave function $\tilde{\Psi}$, so that, for a given nuclei positions, the expectation value of the Hamiltonian in $\tilde{\Psi}$, an upper bound to the true ground state energy, becomes a function of parameters $E = E(p_1, p_2 \ldots p_K)$. Let's guess that the number P of parameters per variable needed for the desired accuracy is $3 \leq P \leq 10$. The energy needs to be minimized in the space of K parameters,

$$K = P^{3N} \ , \qquad 3 \leq P \leq 10 \ . \tag{2.8}$$

Call $\bar{K}$ the maximum value feasible with the best computer software and hardware, and $\bar{N}$ the corresponding maximum number of electrons, then from Eq. (2.8):

$$\bar{N} = \frac{1}{3}\frac{\ln \bar{K}}{\ln P} \ . \tag{2.9}$$

If we take optimistically $\bar{K} \approx 10^9$ and $P = 3$, we obtain the shocking result $\bar{N} = 6$ electrons. The exponential in Eq. (2.8) represents a wall severely limiting $\bar{N}$. If we turn the question around and find what is the needed K for $N = 100$ electrons, taking $P = 3$, we obtain again a shocking result $K \approx 10^{150}$. We conclude that traditional wave-function methods are generally limited to molecules with a small total number of chemically active electrons, usually $N < 10$. DFT provides a viable alternative for larger systems, less accurate perhaps, but much more versatile.

2.2 The Hohenberg-Kohn Formulation of DFT

First theorem of Hohenberg and Kohn The ground-state density $n(\boldsymbol{r})$ of a system of interacting electrons in an external potential $v(\boldsymbol{r})$ determines uniquely this potential, up to an arbitrary constant [21].
In the case of a degenerate ground state, the theorem refers to any ground-state density $n(\boldsymbol{r})$. The proof for a non-degenerate ground state is by contradiction. Suppose there existed two potential $v_1(\boldsymbol{r})$ and $v_2(\boldsymbol{r})$ yielding the same density $n(\boldsymbol{r})$. There corresponds to these potential two different ground-state wave functions Ψ_1 and Ψ_2. Let's consider Ψ_2 as trial wave function for the potential $v_1(\boldsymbol{r})$. Then by the variational principe:

$$\left\langle \Psi_2 | \mathscr{T}_\mathrm{e} + \mathscr{V}_\mathrm{ee} | \Psi_2 \right\rangle + \int n_2(\boldsymbol{r}) v_1(\boldsymbol{r}) d^3r \geq \left\langle \Psi_1 | \mathscr{T}_\mathrm{e} + \mathscr{V}_\mathrm{ee} | \Psi_1 \right\rangle + \int n_1(\boldsymbol{r}) v_1(\boldsymbol{r}) d^3r \,. \tag{2.10}$$

But since both wave functions have the same density:

$$\left\langle \Psi_2 | \mathscr{T}_\mathrm{e} + \mathscr{V}_\mathrm{ee} | \Psi_2 \right\rangle \geq \left\langle \Psi_1 | \mathscr{T}_\mathrm{e} + \mathscr{V}_\mathrm{ee} | \Psi_1 \right\rangle \,. \tag{2.11}$$

But we can exchange wave function 1 with 2, reversing the inequality. This leads to a contradiction, unless the total energy of the two wavefunctions is the same, which implies they are the same wavefunction by the variational principle and the assumption of non-degeneracy. The unique potential $v(\boldsymbol{r})$ can be then determined by inversion of the Schrödinger equation,

$$v(\boldsymbol{r}) = -\frac{1}{2} \sum^{N} \nabla_i^2 \Psi / \Psi + \frac{1}{2} \sum_{i \neq j} \frac{1}{|\boldsymbol{r}_i - \boldsymbol{r}_j|} \,. \tag{2.12}$$

The theorem can be extended to degenerate ground state wave functions by a constrained search method [22]. Let us denote by Ψ_n^α the class of wave functions which yields a certain density $n(\boldsymbol{r})$. Let us define the functional:

$$F[n(\boldsymbol{r})] = \min_\alpha \left\langle \Psi_n^\alpha | \mathscr{T}_\mathrm{e} + \mathscr{V}_\mathrm{ee} | \Psi_n^\alpha \right\rangle \,, \tag{2.13}$$

where the minimization is over all the antisymmetric Ψ_n^α yielding $n(\boldsymbol{r})$. Let us call $\Psi_{\bar{n}}^{\alpha_0}$ the wave-function that minimize $F[n]$ for a certain density $\bar{n}$. $F[n]$

requires no explicit knowledge of the external potential $v(\boldsymbol{r})$, it is an universal functional of the density. The ground-state energy E_0 is then simply,

$$E_0 = \min_n \int v(\boldsymbol{r}) n(\boldsymbol{r}) d^3r + F[n(\boldsymbol{r})] \,, \tag{2.14}$$

where the minimization is over all the positive definite densities $n(\boldsymbol{r})$. Once the ground state density $n_0(\boldsymbol{r})$ has been determined from Eq. (2.14), the unique correspondent potential is built from $\Psi^{\alpha_0}_{n_0}$ through Eq. (2.12).

2.3 The Self-Consistent Kohn-Sham Equations

The Kohn-Sham (KS) equations provide a convenient scheme to determine the ground state energy and density of a system without performing the constrained search in Eq. (2.14), that is computationally very demanding. Let us consider a system of N non-interacting electrons, with ground-state density $n_0(\boldsymbol{r})$, moving in an external potential $v(\boldsymbol{r})$. If we take a trial density $n(\boldsymbol{r})$, it follows

$$E[n(\boldsymbol{r})] = \int v(\boldsymbol{r}) n(\boldsymbol{r}) d^3r + T_s[n(\boldsymbol{r})] \geq E_0 \,, \tag{2.15}$$

where $T_s[n(\boldsymbol{r})]$ is the kinetic energy of the ground state of non-interacting electrons with density $n(\boldsymbol{r})$. The Euler-Lagrange equations are obtained by minimization of functional $E[n(\boldsymbol{r})]$ with respect to density, leaving the particle number unchanged:

$$\frac{\delta T_s[n(\boldsymbol{r})]}{\delta n(\boldsymbol{r})}|_{n=n_0} + v(\boldsymbol{r}) - \varepsilon = 0 \,, \tag{2.16}$$

where $n_0(\boldsymbol{r})$ is the exact ground state density for $v(\boldsymbol{r})$ and ε is a Lagrange multiplier to assure particle number conservation. In the non-interacting case we know that the ground state density and energy can be determined by calculating the eigenfunctions Φ_i and eigenvalues ε_i of non-interacting single-particle equations

$$\left(-\frac{1}{2}\nabla^2 + v(\boldsymbol{r}) - \varepsilon_i \right) \Phi_i(\boldsymbol{r}) = 0 \,. \tag{2.17}$$

Let us now consider the problem of interacting electrons, we can deliberately write the functional $F[n(\boldsymbol{r})]$ in Eq. (2.13) in the form

$$F[n(\boldsymbol{r})] = T_s[n(\boldsymbol{r})] + \frac{1}{2}\int \frac{n(\boldsymbol{r}) n(\boldsymbol{r}')}{|\boldsymbol{r} - \boldsymbol{r}'|} d^3r d^3r' + E_{xc}[n(\boldsymbol{r})] \,, \tag{2.18}$$

where $T_s[n(\boldsymbol{r})]$ is the kinetic energy functional for non-interacting electrons and $E_{xc}[n(\boldsymbol{r})]$ is the so-called exchange-correlation energy functional. The cor-

responding Euler-Lagrange equation for a fixed number of electrons has the following form

$$\frac{\delta T_s[n(\boldsymbol{r})]}{\delta n(\boldsymbol{r})}|_{n=n_0} + v_{\text{eff}}(\boldsymbol{r}) - \varepsilon = 0 \,, \tag{2.19}$$

where

$$v_{\text{eff}}(\boldsymbol{r}) = v(\boldsymbol{r}) + \int \frac{n(\boldsymbol{r}')}{|\boldsymbol{r}-\boldsymbol{r}'|} d^3r' + v_{xc}(\boldsymbol{r}) \tag{2.20}$$

and

$$v_{xc}(\boldsymbol{r}) = \frac{\delta E_{xc}[n(\boldsymbol{r})]}{\delta n(\boldsymbol{r})}|_{n=n_0} \,. \tag{2.21}$$

The form of Eq. (2.19) is identical to that of Eq. (2.16) for non-interacting particles moving in an effective external potential $v_{\text{eff}}(\boldsymbol{r})$, so we conclude that the ground-state density $n_0(\boldsymbol{r})$ can be obtained by solving the single particle equation

$$\left(-\frac{1}{2}\nabla^2 + v_{\text{eff}}(\boldsymbol{r}) - \varepsilon_i\right)\Phi_i(\boldsymbol{r}) = 0 \,, \tag{2.22}$$

with

$$n_0(\boldsymbol{r}) = \sum_{i=1}^{N} |\Phi_i(\boldsymbol{r})|^2 \,. \tag{2.23}$$

The equations (2.20), (2.22) and (2.23) are the so-called KS equations. In practice, they are solved by iteration (self-consistent approach): a form is guessed for the density $n(\boldsymbol{r})$, a potential $v_{\text{eff}}(\boldsymbol{r})$ is then calculated by Eq. (2.20), the KS orbitals are obtained by Eq. (2.22) and finally a new density is calculated by Eq. (2.23). The procedure is continued until further iterations do not materially alter the density or the potential. The ground-state energy is then given by:

$$E_0 = \sum_i \varepsilon_i + E_{xc}[n_0(\boldsymbol{r})] - \int v_{xc}(\boldsymbol{r}) n_0(\boldsymbol{r}) d^3r - \frac{1}{2}\frac{\int n_0(\boldsymbol{r}) n_0(\boldsymbol{r}')}{|\boldsymbol{r}-\boldsymbol{r}'|} \,. \tag{2.24}$$

Ideally, with the exact E_{xc} and v_{xc}, all many-body effects would be in principle included in the calculation.
In conclusion, the many-body problem has been mapped into an effective single-particle problem of an electron moving into an effective potential $v_{\text{eff}}(\boldsymbol{r})$.

2.4 Approximations for the Exchange-Correlation Potential

The simplest and at the same time most successful approximation to $E_{xc}[n(\boldsymbol{r})]$ is the local-density approximation (LDA),

$$E_{xc}^{\mathrm{LDA}} \equiv \int \varepsilon_{xc}(n(\boldsymbol{r}))n(\boldsymbol{r})d^3r\,, \tag{2.25}$$

where $\varepsilon_{xc}(n(\boldsymbol{r}))$ is the exchange-correlation energy per particle of an uniform electron gas of density $n(\boldsymbol{r})$. The exchange part of ε_{xc} is elementary [23], while the correlation part was first estimated in 1934 by E. Wigner [24] and more recently with precision about 1% by Ceperley and Alder [25]. LDA has been found to perform remarkably well for a range of applications incredibly large. Experience has shown that LDA gives ionization energies of atoms, dissociation energies of molecules and cohesive energies with an error typically within 10-20 % [26]. However LDA fails in strongly correlated electron systems, like heavy-fermion materials, since they lack any resemblance to non-interacting electron gases. In many applications an improvement of LDA method is achieved by the generalized gradient approximation (GGA) to $E_{xc}[n(\boldsymbol{r})]$, by means of a functional of the density and its gradients that fulfills a maximum number of exact relations,

$$E_{xc}^{\mathrm{GGA}}[n(\boldsymbol{r})] = \int f(n(\boldsymbol{r}), |\nabla n(\boldsymbol{r}))|d^3r\,. \tag{2.26}$$

In this case the exchange-correlation potential $v_{xc}(\boldsymbol{r})$ in Eq. (2.21) becomes

$$v_{xc}[n(\boldsymbol{r})] = \frac{\delta E_{xc}[n(\boldsymbol{r})]}{\delta n(\boldsymbol{r})} - \nabla \cdot \frac{\delta E_{xc}[n(\boldsymbol{r})]}{\delta \nabla n(\boldsymbol{r})}\,. \tag{2.27}$$

The gradient of the density is usually determined numerically. In practice GGA approximation often improves LDA in the calculations of the structural properties of metals, like equilibrium volume, bulk modulus and transition pressure between solid phases [26]. One of the most common GGA approximation is, for example, the Perdew-Wang-91 functional [27].

3. The APW+lo Basis Set

The practioners of density functional theory are divided in two communities: those that are using plane-waves basis set, mathematically simple and consequently easier to handle in programming but in principle less efficient; and those that are utilizing more complex but more efficient basis sets, such as the linearized muffin-tin orbital (LMTO) and augmented plane-wave (APW) based basis sets. The latter methods do not need a pseudo-potential to treat the electrons closer to the nucleus since they include all electrons explicitly in the calculation. Experience has shown that the all-electron approach is more accurate than pseudo-potentials in treating the properties of d and f-band materials, especially non-collinear magnetism [28, 29].

The APW+lo [30, 31, 32] method is a generalization and improvement of the original APW method of Slater [33]. Hence we will first review the original APW method and explain the motivations that lead to the APW+lo extension.

3.1 APW Method

Slater clearly explains the essence of the APW basis set in his 1937 pioneering paper [33]: near an atomic nucleus the potential and wave-functions are similar to those in an atom, they are strongly varying and almost spherical. In the interstitial space between the atoms both the potential and wave-functions are smoother and slowly varying. Accordingly to this observation, it is convenient to divide space into two regions where different basis expansions are used: radial solutions of Schrödinger's equation inside spheres S_α centered at atom α and planewaves in the remaining interstitial region I. The two sets are then matched at the sphere boundary. Every sphere has a non-overlapping muffin-tin (MT) radius R_α^{MT}. The Kohn-Sham wave-function is then expanded over basis functions $\phi_{\boldsymbol{k}+\boldsymbol{G}}(\boldsymbol{r})$ defined by

$$\phi_{\boldsymbol{k}+\boldsymbol{G}}(\boldsymbol{r}) = \frac{1}{\sqrt{\Omega}} e^{i\boldsymbol{k}\cdot\boldsymbol{r}} \quad \text{for} \quad \boldsymbol{r} \in I \,, \tag{3.1}$$

$$\phi_{\boldsymbol{k}+\boldsymbol{G}}(\boldsymbol{r}) = \sum_{\alpha\ell m} A_{\ell m}^{\alpha}(\boldsymbol{k}+\boldsymbol{G}) u_{\ell m}(r_\alpha) Y_{\ell m}(\hat{r}_\alpha) \quad \text{for} \quad \boldsymbol{r} \in S_\alpha \,. \tag{3.2}$$

Here Ω is the unit cell volume, $\boldsymbol{r}_\alpha = \boldsymbol{r} - \boldsymbol{R}^\alpha$, with $\boldsymbol{R}^\alpha$ position of the sphere α, $A^\alpha_{lm}(\boldsymbol{k}+\boldsymbol{G})$ are the matching coefficients, $Y_{\ell m}(\hat{r}_\alpha)$ are spherical harmonics, and, finally, $u_{\ell m}(r_\alpha)$ are solutions of the radial Schrödinger equation:

$$\Big[-\frac{d^2}{dr_\alpha^2} + \frac{\ell(\ell+1)}{r_\alpha^2} + v_{\text{eff},\alpha}(r_\alpha) - E_\ell\Big] r u_\ell(r_\alpha) = 0\ . \tag{3.3}$$

Here $v_{\text{eff},\alpha}$ refers to the spherical component of the effective KS potential inside the sphere α, E_ℓ is a parameter. In order to determine the matching coefficients we expand Eq. (3.1) with Rayleigh formula,

$$e^{i\boldsymbol{k}\cdot\boldsymbol{r}_\alpha} = 4\pi \sum_{lm} i^l j_\ell(kr_\alpha) Y_{\ell m}(\hat{r}_\alpha) Y^*_{\ell m}(\hat{k})\ , \tag{3.4}$$

where $j_\ell(kr_\alpha)$ are spherical Bessel functions and $\boldsymbol{r}_\alpha$ is a point on the surface of the sphere. We write $e^{i\boldsymbol{k}\cdot\boldsymbol{r}} = e^{i\boldsymbol{k}\cdot\boldsymbol{R}_\alpha} e^{i\boldsymbol{k}\cdot\boldsymbol{r}_\alpha}$, we multiply Eq. (3.4) by $Y^*_{\ell m}(\hat{r}_\alpha)$ and we integrate over the sphere. Inside the MT sphere we use Eq. (3.2), again we multiply by $Y^*_{\ell m}(\hat{r}_\alpha)$ and we integrate over the sphere. Finally the continuity of the basis functions $\phi_{\boldsymbol{k}}(\boldsymbol{r})$ at the sphere boundary gives us the following condition for the matching coefficients:

$$A^\alpha_{lm}(\boldsymbol{k}+\boldsymbol{G}) = \frac{4\pi}{\sqrt{\Omega}} \frac{i^\ell j_\ell((k+G)R^{\text{MT}}_\alpha) Y^*_{\ell m}(\widehat{k+G})}{u_\ell(R^{\text{MT}}_\alpha)}\ . \tag{3.5}$$

If E_ℓ is taken as a fixed parameter, rather than a variational coefficient, the APW method would simply amount to the use of the APWs as a basis. This would result in a secular equation,

$$\det[H - EO(E)] = 0\ , \tag{3.6}$$

that is non-linear in energy. Here H and O refer, respectively, to the Hamiltonian and the overlap matrix (the APW are not orthogonal hence O is non trivial). The solution of this secular equation would then yield the band energies and wave-functions, but only at the energy E_ℓ. The lack of variational freedom does not allow for changes in the wavefunction as the band energy deviates from this reference. Accordingly, E_ℓ must be set equal to the band energy. This means that the energy bands at a fixed k-point cannot be obtained from a single diagonalization of Eq. (3.6). Rather it is necessary to determine the secular determinant as function of energy and determine its roots, and this a very computationally demanding procedure. A short-cut to this procedure is given by the method of meta-eigenvalues of Sjöstedt and Nordström [34], but still it would be needed more than one diagonalization of the secular matrix for every k-point.

3.2 Introduction of Local Orbitals

The secular equation Eq.(3.6) can be linearized by adding some local orbitals [30] (lo) to the APW basis functions,

$$\phi_{\mathrm{lo}}(\boldsymbol{r}) = 0 \ \text{ for } \ \boldsymbol{r} \in I \ , \tag{3.7}$$

$$\phi_{\mathrm{lo}}(\boldsymbol{r}) = [a^{\alpha}_{\ell m} u^{\alpha}_{\ell}(r_{\alpha}) + b^{\alpha}_{\ell m} \dot{u}^{\alpha}_{\ell}(r_{\alpha})] Y_{\ell m}(\hat{r_{\alpha}}) \ \text{ for } \ \boldsymbol{r} \in S_{\alpha} \ . \tag{3.8}$$

Here $\dot{u}(r_{\alpha})$ refers to the spatial derivative of the solution $u(r_{\alpha})$ of the radial Schrödinger equation. Usually the lo's are evaluated at the same fixed energy E_{ℓ} of the corresponding APW's. The addition of these function removes the strong energy dependence of the matrices H and O by making the secular equation linear in energy within a certain region. All eigenvalues within this region can then be found from a single diagonalization of the secular matrix. The error in this procedure is of the order $(\varepsilon - \varepsilon_0)^2$ for the wavefunction, and, consequently it goes $(\varepsilon - \varepsilon_0)^4$ for the band energies, where ε and ε_0 indicate, respectively, the chosen linearization energy and the exact solution. Finally, the choice of the appropriate set of lo's in the semi-core energy region (at the boundary between the lowest lying states, the so-called core states, and the valence ones) increases the flexibility of the basis set such that the semi-core states are correctly described [31].

3.3 Treatment of Core Electrons

For large atoms with many electrons, the core states are well localized inside the MT spheres. The APW+lo method is an all-electron method, this means that the core electrons state are not replaced by a pseudo-potential but they are explicitly included in the calculation [28]. The high kinetic energy of these core electrons makes relativistic effects important and instead of solving the Schrödinger equation for these states, we solve the Dirac equation with only the spherical part of the potential. At the sphere boundary the core wavefunctions and their derivatives are assumed to vanish. Also the core wavefunctions are assumed to be orthogonal to any valence state.

4. Intra-atomic Non-collinear Magnetism

4.1 Spin-dependent DFT

Density functional theory has been generalized to the spin-dependent case by Von Barth and Hedin [35]: the density $\rho(\boldsymbol{r})$ becomes a 2x2 matrix

$$\rho(\boldsymbol{r}) = \frac{(n(\boldsymbol{r})\mathscr{I} + \boldsymbol{m}\cdot\boldsymbol{\sigma})}{2}\ , \tag{4.1}$$

where $\mathscr{I}$ is the 2x2 identity matrix and $\boldsymbol{\sigma} = (\sigma_x, \sigma_y, \sigma_z)$ refers to the Pauli matrices. The new physical quantity, beside the charge density $n(\boldsymbol{r})$, is the vector magnetization density $\boldsymbol{m}(\boldsymbol{r})$. The effective Kohn-Sham (KS) potential, which has been defined through functional derivatives of the total energy functional by respect to the density, also becomes a 2x2 matrix,

$$V_{\text{eff}}(\boldsymbol{r}) = v_{\text{eff}}(\boldsymbol{r})\mathscr{I} - \boldsymbol{b}(\boldsymbol{r})\cdot\boldsymbol{\sigma}. \tag{4.2}$$

The non-magnetic part of the potential $v_{\text{eff}}(\boldsymbol{r})$ includes the Hartree term, the nuclei attraction and the exchange-correlation potential $v_{xc}(\boldsymbol{r})$, while the magnetic potential $\boldsymbol{b}(\boldsymbol{r})$ only receives contributions from the exchange-correlation functional. In the spin-polarized version of LDA approximation the exchange-correlation functional is expressed as [35]

$$E_{xc}[n(\boldsymbol{r}), \boldsymbol{m}(\boldsymbol{r})] = \int n(\boldsymbol{r})\varepsilon_{xc}(n(\boldsymbol{r}), |\boldsymbol{m}(\boldsymbol{r})|)d^3r\ , \tag{4.3}$$

where $\varepsilon_{xc}(n,m)$ is the exchange-correlation density for a spin-polarized homogeneous electron gas with charge density n and magnetization density of magnitude m. The functional form of $\varepsilon_{xc}(n,m)$ has been parametrized in different ways [35, 25, 36]. The non-magnetic scalar exchange correlation potential is derived from LDA exchange correlation energy as

$$v_{xc}(\boldsymbol{r}) = \frac{\delta E_{xc}}{\delta n(\boldsymbol{r})} = \varepsilon_{xc}(n(\boldsymbol{r}), |\boldsymbol{m}(\boldsymbol{r})|) + n(\boldsymbol{r})\Big[\frac{\partial \varepsilon_{xc}(n,m)}{\partial n}\Big]_{n=n(\boldsymbol{r}), m=|\boldsymbol{m}(\boldsymbol{r})|}\ , \tag{4.4}$$

and the magnetic potential, which now assumes the form of a magnetic field, is derived as

$$\boldsymbol{b}(\boldsymbol{r}) = -\frac{\delta E_{xc}}{\delta \boldsymbol{m}(\boldsymbol{r})} = -\hat{\boldsymbol{m}}(\boldsymbol{r})n(\boldsymbol{r})\Big[\frac{\partial \varepsilon_{xc}(n,m)}{\partial m}\Big]_{n=n(\boldsymbol{r}), m=|\boldsymbol{m}(\boldsymbol{r})|}\ , \tag{4.5}$$

where $\hat{m}(\boldsymbol{r}) = \frac{\delta|\boldsymbol{m}(\boldsymbol{r})|}{\delta \boldsymbol{m}(\boldsymbol{r})}$ is the direction of the magnetization density vector at the point $\boldsymbol{r}$. As it is clear from Eq. (4.5), the potential $\boldsymbol{b}(\boldsymbol{r})$ is constructed to be parallel to the magnetization density $\boldsymbol{m}(\boldsymbol{r})$ at every point.
In the spin-polarized case the KS Hamiltonian [37] is expressed as

$$H = [-\nabla^2/2 + V_{\text{eff}}(\boldsymbol{r})]\mathscr{I} - \boldsymbol{b}(\boldsymbol{r}) \cdot \boldsymbol{\sigma} \ . \tag{4.6}$$

The charge density and magnetization are constructed by summing over the occupied states,

$$n(\boldsymbol{r}) = \sum_{i}^{\text{occ}} \Phi_i^{\dagger}(\boldsymbol{r})\Phi_i(\boldsymbol{r}) \tag{4.7}$$

and

$$\boldsymbol{m}(\boldsymbol{r}) = \sum_{i}^{\text{occ}} \Phi_i^{\dagger}(\boldsymbol{r})\sigma\Phi_i(\boldsymbol{r}) \ , \tag{4.8}$$

where Φ_i are the eigenfunctions of the Hamiltonian in Eq. (4.6). A self-consistent (SC) solution of the problem is obtained when the input charge and magnetization density produce the same output charge and magnetization density. We emphasize that also the non-collinearity of the magnetization density is given by this SC procedure. This approach to non-collinear magnetism is the most general, i.e. the magnetization density is treated as a continuous vector both in direction and magnitude at every point in space [29]. In Fig. 4.1 , as example, we show the non-collinear magnetization density in US. Collinear magnetism can be interpreted as a special case in which the magnetization density is parallel, at every point, to a global direction $\hat{e}$. In this case we can define spin-up and spin-down potentials and the KS Hamiltonian in Eq. (4.6) can be transformed into a block diagonal form.

4.2 Spin-spirals

The formalism described above is applicable to cases where the magnetic unit cell is identical to the unit cell utilized in the calculation. Herring [38] has shown that non commensurate helical or cyclic waves, often referred as spin-spirals, can be treated with the chemical unit cell, instead of the magnetic one. This approach is valid only if the spin space can be decoupled to the lattice, or real space, i.e. if the spin-orbit coupling (SOC) interaction can be neglected [39]. A spin-spiral with wave-vector $\boldsymbol{q}$ is defined by its translational properties,

$$\mathscr{T}\boldsymbol{m}(\boldsymbol{r}) = \boldsymbol{m}(\boldsymbol{r}+\boldsymbol{R}) = \mathscr{R}(\boldsymbol{q}\cdot\boldsymbol{R})\boldsymbol{m}(\boldsymbol{r}) \ , \tag{4.9}$$

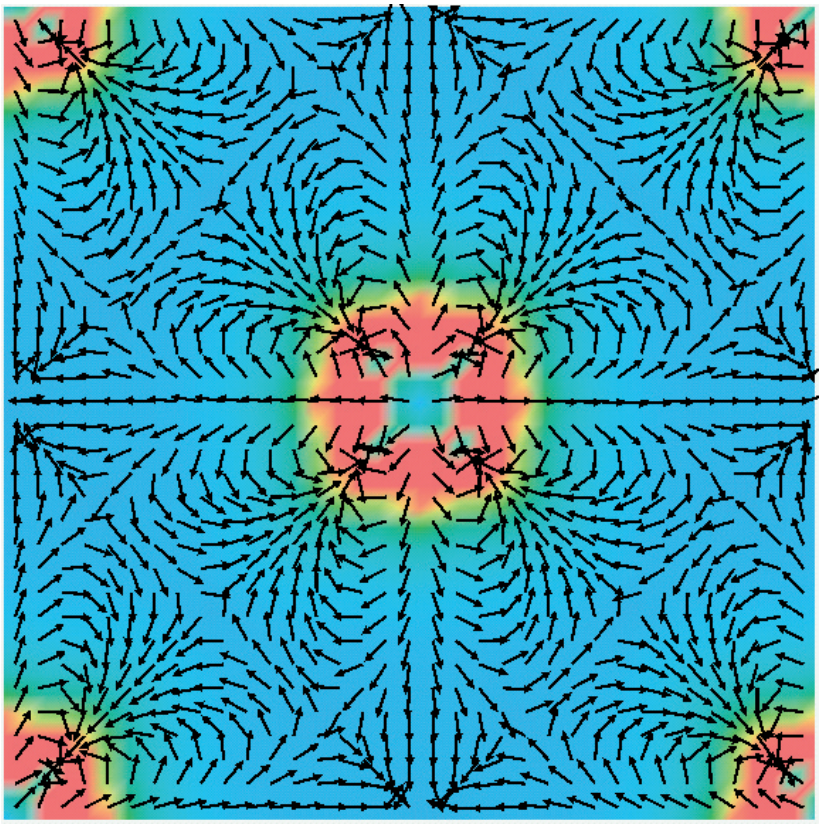

Figure 4.1: Magnetization density in xy plane, $\boldsymbol{m}_{xy}(\boldsymbol{r})$, of the cubic cell of US, $a = 10.36$ a.u., with moments along [001] calculated with LDA+U method. The slice corresponds to $z = 0.55a$ and the U atom is at the center of the cell. The arrows indicate the direction of $\boldsymbol{m}_{xy}(\boldsymbol{r})$ and the colors indicate its magnitude, with red and blue referring, respectively, to the largest and smallest value. The magnetization density is treated as a continuos vector field [29].

where $\mathscr{R}(\phi)$ is a rotation by the angle $\phi = \boldsymbol{q}\cdot\boldsymbol{R}$ around a certain axis and $\boldsymbol{R}$ is a lattice vector. It is convenient to take such axis parallel to $\boldsymbol{q}$ in real space and parallel to z in spin space; we are allowed to do that since spin and real space are not coupled in absence of SOC interaction. The x and y components of the magnetization will continuously rotate while the spiral propagates along $\boldsymbol{q}$. If the z component of the magnetization is zero, we will refer to the spiral as planar, otherwise as conical. We now introduce a generalized translation operator, $\mathscr{T}_{\mathscr{R}} = \mathscr{R}^{-1}\mathscr{T}$ such that $\mathscr{T}_R\boldsymbol{m}(\boldsymbol{r}) = \boldsymbol{m}(\boldsymbol{r})$. This relation will also hold for the magnetic field $\boldsymbol{b}(\boldsymbol{r})$, that is constructed to be parallel to $\boldsymbol{m}(\boldsymbol{r})$ at every point. In order to make efficiently use of fast Fourier transforms it is convenient to define new complex densities $u(\boldsymbol{r})$ and $h(\boldsymbol{r})$ [29], which are invariant under translation $\mathscr{T}$ by construction,

$$u(\boldsymbol{r}) = e^{-i\boldsymbol{q}\cdot\boldsymbol{r}}[m_x(\boldsymbol{r}) + im_y(\boldsymbol{r})] \tag{4.10}$$

and

$$h(\boldsymbol{r}) = e^{-i\boldsymbol{q}\cdot\boldsymbol{r}}[b_x(\boldsymbol{r}) + ib_y(\boldsymbol{r})]. \tag{4.11}$$

The KS Hamiltonian is rewritten in terms of these new densities

$$\mathscr{H} = [-\nabla^2/2 + v_{\text{eff}}(\boldsymbol{r})]\mathscr{I} - [e^{i\boldsymbol{q}\cdot\boldsymbol{r}}h(\boldsymbol{r})\sigma_- + H.c.] - b_z(\boldsymbol{r})\sigma_z, \tag{4.12}$$

where $\sigma_\pm = \frac{1}{2}(\sigma_x \pm i\sigma_y)$. This Hamiltonian is diagonalized by the generalized Bloch spinors [38]

$$\Phi_{j\boldsymbol{k}}(\boldsymbol{r}) = \begin{pmatrix} e^{i(\boldsymbol{k}-\boldsymbol{q}/2)\cdot\boldsymbol{r}}\alpha_{jk}(\boldsymbol{r}) \\ e^{i(\boldsymbol{k}+\boldsymbol{q}/2)\cdot\boldsymbol{r}}\beta_{jk}(\boldsymbol{r}) \end{pmatrix}, \tag{4.13}$$

where α and β are translationally invariant functions. From these wavefunctions we can construct the new densities [29], for example

$$u(\boldsymbol{r}) = \sum_{j\boldsymbol{k}}^{\text{occ}} \Phi^\dagger_{j\boldsymbol{k}}[2e^{-i\boldsymbol{q}\cdot\boldsymbol{r}}\sigma_+]\Phi_{j\boldsymbol{k}}. \tag{4.14}$$

In Fig. 4.2 we show an example of SC spin-spiral calculation for Fe-fcc by applying the method described above that we implemented in the full-potential APW+lo code Elk [40].

4.3 Spin-orbit Interaction

The SOC term is important for the band structure and many properties of materials containing heavier elements, as well as for some properties, like the magneto-crystalline anisotropy, of lighter magnetic materials. The corresponding SOC interaction that enters in the KS Hamiltonian is [41, 42, 43]:

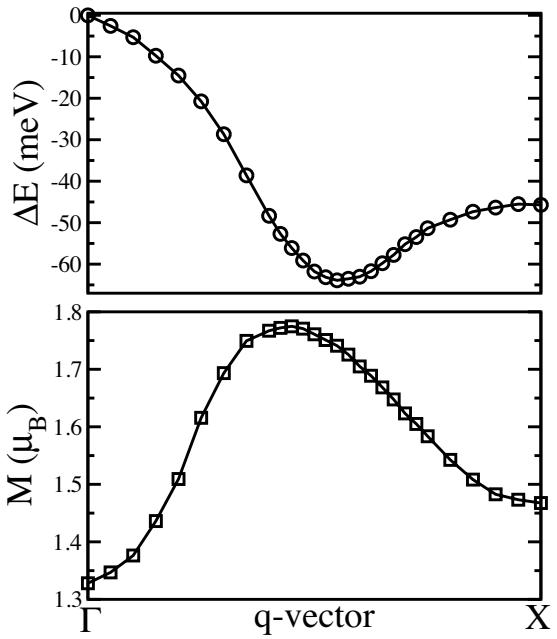

Figure 4.2: Energy difference (upper panel) and magnetic moment (lower panel) of planar spin-spirals in Fe-fcc, $a = 6.82$ a.u., as function of the spin-spiral wave vector $\boldsymbol{q}$.

$$\mathscr{H}_{\mathrm{SOC}} = \xi(r)\boldsymbol{l}\cdot\boldsymbol{s} = \frac{1}{2\alpha}\left(\frac{1}{r}\frac{dv_{\mathrm{eff}}(r)}{dr}\right)\boldsymbol{l}\cdot\boldsymbol{s}\,. \tag{4.15}$$

Here α is the fine structure constant, v_{eff} is the spherical part of the KS effective potential and $\boldsymbol{l}$ and $\boldsymbol{s}$ are, respectively, the single particle spin and angular momentum operators. There is some ambiguity about whether or not include the contribution from the exchange potential v_{xc} in the calculation of SOC parameter $\xi(r)$. However, in practice, the consequences of doing this are negligible and we decide to include it [41].

The term $\mathscr{H}_{\mathrm{SOC}}$ can be rewritten by using the raising (lowering) spin and angular momentum operators, respectively, l^+ (l^-) and s^+ (s^-),

$$\mathscr{H}_{\mathrm{SOC}} = \frac{1}{4\alpha}\left(\frac{1}{r}\frac{dv_{\mathrm{eff}}(r)}{dr}\right)(l^-s^+ + l^+s^- + 2l_zs_z). \tag{4.16}$$

The SOC interaction couples spin-up and spin-down terms, i.e. a calculation including SOC interaction has to necessarily include off-diagonal spin elements in the Hamiltonian.

In APW+lo method the SOC interaction is only applied inside the MT sphere, where the basis function are expanded in spherical harmonics. An example

of band structure calculated with SOC interaction is shown in Fig 4.3 for $PuCoGa_5$, where we can clearly observe an energy split between the $j = 5/2$ and $j = 7/2$ states of the order of 1 eV.

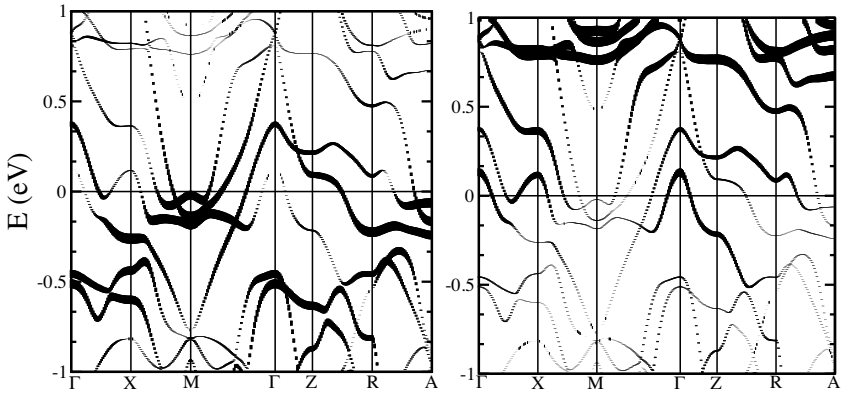

Figure 4.3: Band structure of PuCoGa5 in AF-1$\boldsymbol{k}$, $\boldsymbol{k} = (0,0,1/2)$, calculated with LDA approximation. The fatness of bands indicates the amount of $j = 5/2$ character (left panel) and $j = 7/2$ character (right panel). The zero of the energy is set at the Fermi level.

4.4 Second-variational Approach to Magnetism

The non-magnetic KS Hamiltonian is set up with the full basis set of dimension N (first-variational step). Once this Hamiltonian is diagonalized, only $n \ll N$ states per spin channel are retained to set up the spin-polarized Hamiltonian (second-variational step) [28] with the inclusion of eventual SOC and LDA+U terms. Since the matrix diagonalization time scales like the cube of the matrix dimension, this method becomes computationally very convenient, especially in a non-collinear calculation where spin-up and spin-down wavefunctions are coupled, as we show in Tab. 4.1. By adopting this approach we are assuming that magnetism, SO coupling and LDA+U terms are perturbative corrections to the non-magnetic Hamiltonian, i.e. that the new solution can be well described with only a subset of the first-variational eigenvectors. As it is shown in Fig. 4.4, the dimension of this subset n is a convergence parameter that has to be checked in the calculation.

Table 4.1: *Comparison of time-scaling of Hamiltonian diagonalization in a calculation that makes use of the second-variational step and in one that performs a full diagonalization in a single step. N indicates the full dimension of the basis set, while n is the number of states per spin that are retained in the second-variational step.*

Collinear calculation	
Full diagonalization in one step	Second-variational approach
$2N^3$	$N^3 + 2n^3$
Non-collinear calculation	
Full diagonalization in one step	Second-variational approach
$(2N)^3$	$N^3 + (2n)^3$

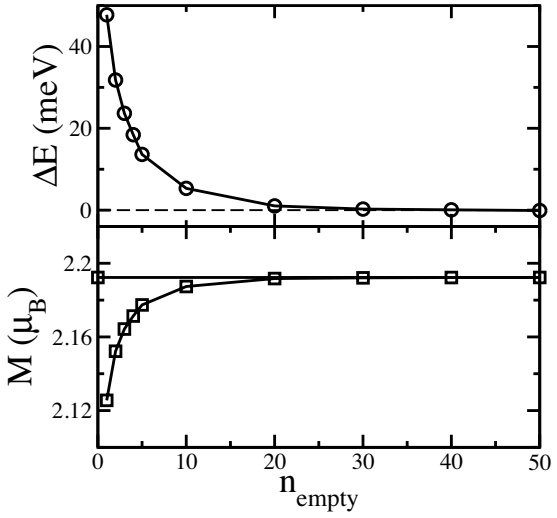

Figure 4.4: Convergence of total energy and magnetic moment in Fe bcc, $a = 5.416$ a.u., by respect to parameter n_{empty} that governs the dimension of the second-variational Hamiltonian. The number n of second-variational states per spin is $n = n_{\text{val}}/2 + n_{\text{empty}}$, where $n_{\text{val}} = 16$ is the valence charge used for Fe.

4.5 Fixed Spin Moment Calculations

An effective magnetic field, $\boldsymbol{b}_{\mathrm{FSM}}$, is required for fixing the spin moment to a given value $\boldsymbol{M}_{\mathrm{FSM}}$ in the MT sphere or in the whole cell. This field is determined by adding a vector to the field which is proportional to the difference between the moment calculated in the ith self-consistent loop, $\boldsymbol{M}^i$, and the required moment $\boldsymbol{M}_{\mathrm{FSM}}$:

$$\boldsymbol{b}_{\mathrm{FSM}}^{i+1} = \boldsymbol{b}_{\mathrm{FSM}}^{i} + \gamma\left(\boldsymbol{M}^i - \boldsymbol{M}_{\mathrm{FSM}}\right), \tag{4.17}$$

where γ is a parameter to be adjusted in order to optimize the convergence. For example, the total energy as function of collinear $\boldsymbol{M}_{\mathrm{FSM}}$ for NiO is plotted in Fig. 4.5, where the minimum corresponds to $M = 1.73\ \mu_B$ in agreement with a non-constrained calculation.

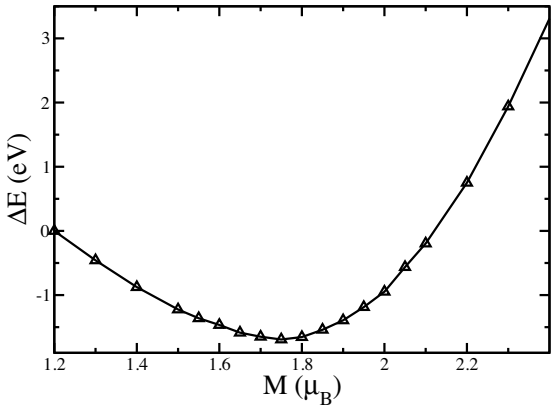

Figure 4.5: Total energy as function of constrained spin moment in NiO AF-II magnetic structure, $a = 7.89$ a.u., treated with LDA+U method (U=8 eV and J=0.9 eV). Here the the convergence parameter γ in Eq. 4.17 is set equal to 0.01.

5. A General Form of LDA+U Method

In the following chapter we will introduce the LDA+U scheme with one single parameter and introduce its multipole decomposition, for reference see also paper II.

In the most general version of LDA+U method [10, 9, 44], an Hartree-Fock (HF) correction to the energy enters with the form

$$E_{\mathrm{HF}} = \frac{1}{2} \sum_{abcd} \rho_{ac} \left[\langle ab|g|cd\rangle - \langle ab|g|dc\rangle \right] \rho_{bd} \ , \tag{5.1}$$

where ρ_{ab} is one element of the density matrix with dimension $D = 2[\ell]$, with $[\ell] = 2(\ell+1)$, which acts as an occupation matrix and a, b, c and d are single electron states. The interaction term is of the form

$$\langle ab|g|cd\rangle = \int \psi_a^\dagger(1)\psi_b^\dagger(2) g(r_{12}) \psi_c(1)\psi_d(2)\mathrm{d}(1)\mathrm{d}(2) \ , \tag{5.2}$$

with one-electron states a with wavefunction $\psi_a(1) = R_\ell(r_1)Y_{\ell m_a}(\Omega_1)\chi_{s_a}(1)$, where the relevant quantum numbers, m and s, are the magnetic quantum number and spin component, respectively. The interaction can be expanded in a series

$$g(r_{12}) = \sum_{k=0}^{\infty} g_k(r_1, r_2) P_k(\cos\theta_{12}) \ , \tag{5.3}$$

where the Legendre function P_k in turn can be expanded by the use of the addition theorem for spherical harmonics

$$P_k(\cos\theta_{12}) = \frac{4\pi}{2k+1} \sum_{q=-k}^{k} Y_{kq}^*(\Omega_1) Y_{kq}(\Omega_2) \ . \tag{5.4}$$

5.1 Slater Integrals Screened by Yukawa Potential

The radial part of the interaction is then contained in the Slater integrals

$$F^{(k)} = \int dr_1 r_1^2 R_\ell^2(r_1) g_k(r_1, r_2) R_\ell^2(r_2) r_2^2 dr_2 \ . \tag{5.5}$$

For a f shell there are four independent parameters, $F^{(0)} = U$, $F^{(2)}$, $F^{(4)}$ and $F^{(6)}$. It is very unpractical to stay with these four parameters. A common practice within LDA+U or HF calculations [9, 44, 45] is to have the screened Slater parameters determined by the choice of two linear combinations of parameters, U and J, and by fixing two ratios, $A_1 = F^{(4)}/F^{(2)}$ and $A_2 = F^{(6)}/F^{(2)}$. In the present work we will instead follow the ideas of Norman [46] and calculate the Slater parameters directly from a screened Coulomb interaction in the form of a Yukawa potential $g(r_1, r_2) = e^{-\lambda r_{12}}/r_{12}$. Then

$$g_k(r_1, r_2, \lambda) = -[k]\lambda\, j_k(i\lambda r_<) h_k^{(1)}(i\lambda r_>) \,, \tag{5.6}$$

where j_k is a spherical Bessel function, $h_k^{(1)}$ is spherical Hankel function of the first kind and $r_<$ and $r_>$ are, respectively, the smaller and the larger radius entering in the double integral in Eq. (5.5). This type of approach has two advantages; it determines the ratio between the different Slater parameters in a more physical way than by choosing U and J individually, and there is only one independent parameter, the screening length λ. Since in the APW+lo basis set $R_\ell(r, \varepsilon)$ is energy dependent, we decide to use the energy ε at the center of the band of the localized shell ℓ. We also set the atomic muffin-tin (MT) radius to a value large enough such that the integrals in Eq. (5.5) are well converged. In the upper part of Fig. 5.1 we plot the calculated Slater parameters for US. These values are in perfect agreement with ones calculated for the ion U^{4+} by Norman [46] with the same screened potential. In the lower part of Fig. 5.1 we compare the Slater integrals ratios A_1 and A_2 obtained for US with the fixed ratios commonly used in most LDA+U studies [9, 47]. There is a good agreement only at small values of the screening length. For $\lambda \geq 0.5$ a.u.$^{-1}$ there start to be a significative difference that turns out to be relevant in the calculation of magnetic moments of US. If the $F^{(k)}$s are calculated individually with Eq. (5.5) and Eq. (5.6), the spin moment ($M_{\rm sp}$) and orbital moment (M_{orb}) show a more dramatic variation as function of U (or λ) than ones determined by fixing A_1 and A_2 to values of Ref. [9, 47] (see Fig. 5.2). This fact indicates how relevant the individual determination of every Slater integral might be in many systems. Finally, another advantage of this approach is that in the limit of large λ one recovers the LDA results. Another parameter-free method to screen the Slater parameter has been suggested by Brooks [48], where the screening parameter λ is identified as the Thomas-Fermi screening, which depends on the local charge density. A more accurate but time-consuming way to calculate the Slater parameters from the screened Coulomb potential is within the RPA approach, as it has been recently accomplished by Solovyev in Ref. [49].

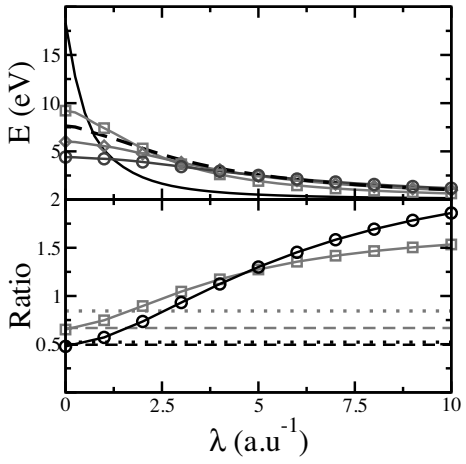

Figure 5.1: Upper panel: Slater parameters $F^{(0)}$ (full black line), $F^{(2)}$ (red line with squares), $F^{(4)}$ (green line with diamonds), $F^{(6)}$ (blue line with circles) and parameter J times 10 (dashed black line) as function of screening length λ of the Yukawa potential in US. Lower panel: comparison of Slater parameters ratios $A_1 = F^{(4)}/F^{(2)}$ (red lines) and $A_2 = F^{(6)}/F^{(2)}$ (black lines) calculated by a screened Yukawa potential (full line with squares for A_1, full line with circles for A_2) with the fixed ones of Ref. [9, 47] (full line for A_1, dashed line for A_2) and of Ref. [45, 46] (dashed-dotted line for A_1, dotted line for A_2).

5.2 Calculation of LDA+U Potential

The contribution to the orbital potential from the LDA+U correction is defined as

$$V_{ij} = \frac{\delta E_{HF}}{\delta \rho_{ji}} = \sum_{ab} \left[\langle ja|g|ib\rangle - \langle ja|g|bi\rangle \right] \rho_{ab} \ . \tag{5.7}$$

We note that the potential so defined is the complex conjugate of the one sometimes stated in literature.The correct definition becomes crucial to evaluate off-diagonal spin terms in all calculations in which the coordinate system is not rotated to the local one, i.e. in all calculations in which the density matrix is not diagonal.

5.3 Double-Counting Corrections

A major obstacle in the LDA+U approach is that the electron-electron interaction has already been included in LDA potential, thus a simple addition of the orbital dependent HF potential would lead to DC terms. One may want to individuate those terms in the LDA potential that correspond to the interaction already considered in the HF Hamiltonian and subtract them. A direct con-

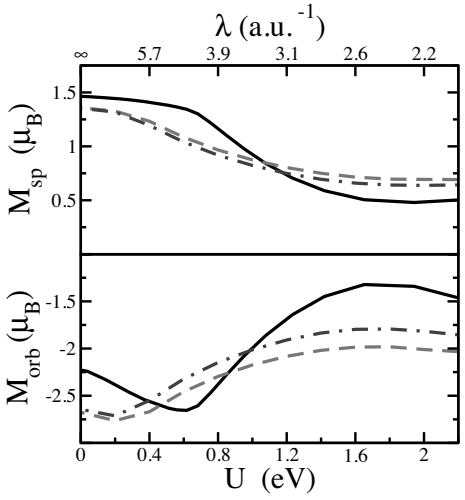

Figure 5.2: Spin (upper panel) and orbital magnetic moment (lower panel) of US, $a = 10.36$ a.u., calculated with LDA+U approach and INT DC (see section 5.3). We compare the results obtained by calculating the $F^{(k)}$s with a screened Yukawa potential (full black line, screening length in the upper axis) with ones obtained by fixing the ratios A_1 and A_2 to ones of Ref. [9, 47] (dashed red line) and to ones of Ref. [45, 46] (dashed-dotted blue line). In the fixed ratios calculations we fixed the parameter J=0.46 eV to one of Ref. [45].

nection between the two formalisms is not possible and in addition it would not be useful. In fact LDA approximation treats very accurately spatial variations of the Hartree and exchange correlation potential but it neglects the orbital dependence of the Coulomb interaction. Thus the best recipe would be to identify the mean-field part of the HF potential and subtract it, leaving only an orbital dependent correction to the mean-field type LDA potential. Czyżyk and Sawatzky [50] suggested a prescription that is exact in the case of uniform occupancies (around-mean-field, AMF) and that would be realistic for weakly correlated systems, however not exact because of the presence of the crystalline field. The AMF correction is implemented by redefining a new density matrix without the charge n and the magnetization $\boldsymbol{m}$ contributions

$$n = \mathrm{Tr}\,\rho \tag{5.8}$$

$$\boldsymbol{m} = \mathrm{Tr}\,\boldsymbol{\sigma}\rho\ , \tag{5.9}$$

in the following way

$$\tilde{\rho}_{ab} = \rho_{ab} - (\delta_{ab} n + \boldsymbol{\sigma}_{ab}\cdot\boldsymbol{m})/D\ . \tag{5.10}$$

The AMF-double-counting corrected LDA+U energy and potential terms become in our formalism

$$E_{HF-\mathrm{dc}}^{\mathrm{AMF}} = \frac{1}{2}\sum_{abcd}\tilde{\rho}_{ac}\left[\langle ab|g|cd\rangle - \langle ab|g|dc\rangle\right]\tilde{\rho}_{bd}\ , \tag{5.11}$$

$$\begin{aligned} V_{ij}^{\mathrm{AFM}} =& V_{ij} - \sum_{ab}\left[\langle ja|g|ib\rangle - \langle ja|g|bi\rangle\right](\delta_{ab}n + \boldsymbol{\sigma}_{ab}\cdot\boldsymbol{m})/D = \\ & \sum_{ab}\left[\langle ja|g|ib\rangle - \langle ja|g|bi\rangle\right]\tilde{\rho}_{ab}\ . \end{aligned} \tag{5.12}$$

For strongly correlated systems it exists another prescription, the fully-localized-limit (FLL) double-counting [9], that would correspond to subtract the average effect for a localized state, with integer occupation number. The most general expressions for energy and potential are

$$E_{\mathrm{dc}}^{\mathrm{FLL}} = \left\{2Un(n-1) - 2Jn(n/2-1) - J\boldsymbol{m}\cdot\boldsymbol{m}\right\}/4\ , \tag{5.13}$$

$$V_{ij}^{\mathrm{FLL}} \quad = \quad V_{ij} - \left[\frac{U(2n-1)}{2} - \frac{J(n-1)}{2}\right]\delta_{ij} + \frac{J\boldsymbol{m}\cdot\boldsymbol{\sigma}_{ij}}{2}\ . \tag{5.14}$$

Most of LDA+U calculations use one of these approaches, while the real occupation numbers lie somewhere between the two limits. Petukhov et al. [12] proposed a linear interpolation between these two limits (INT DC),

$$E_{HF-\mathrm{dc}}^{\mathrm{INT}} = \alpha E_{U-\mathrm{dc}}^{\mathrm{FLL}} + (1-\alpha)E_{U-\mathrm{dc}}^{\mathrm{AMF}}\ , \tag{5.15}$$

$$V_{ij}^{\mathrm{INT}} = \alpha V_{ij}^{\mathrm{FLL}} + (1-\alpha)V_{ij}^{\mathrm{AMF}}\ , \tag{5.16}$$

in which the parameter α is a material dependent constant determined in a self-consistent (SC) way following a constrained-DFT philosophy. In our formalism the expression of α of Ref. [12] is generalized to take into account the off-diagonal spin terms of the density matrix,

$$\alpha = \frac{D\,\mathrm{Tr}\,\tilde{\rho}^2}{Dn - n^2 - m^2}\ , \tag{5.17}$$

where n and m are defined in Eq. (5.8).

In the present study we prefer to use the INT DC approach for two reasons. Firstly, it reduces one further free parameter. The results do depend on the choice of DC, but if we stay consequently with the INT DC this degree of freedom is gone since we can in principle treat both more itinerant and more localized system. Secondly, it turns out that the use of the INT DC is very important to reproduce the correct magnetic structure of monopnictides Pu compounds. In Fig. 5.3 we compare M_{sp} and M_{orb} calculated for the fer-

romagnetic PuS [51] with ones calculated for the paramagnet PuP [51]. For AMF type of DC, M_{sp} and M_{orb} of both compounds decrease dramatically until they disappear at $U \approx 2.0$ eV. Instead, by using FLL DC, M_{sp} and M_{orb} decrease significantly but they never disappear for any value of U. Finally, only by using the INT type of DC, we find a range of values for U ($U \gtrsim 4.0$ eV) in which PuS is magnetic and PuP is non-magnetic. In conclusion we have implemented the LDA+U method in the most general form in the full-potential APW+lo code ELK [40], taking into account the off-diagonal spin terms of the density matrix and the correct definition of the potential for those terms. By using the interpolated DC of Petukhov et al. [12] and by calculating SC the $F^{(k)}$s with a Yukawa potential, our LDA+U approach has only one free parameter left, i.e. the screening length λ, or if preferable U.

5.4 Multipole Representation of LDA+U Energy

The formalism up to now is standard and have been used several times before, although some studies have neglected the spin-mixing terms in Eq. (5.1). Within this formalism the density matrix plays a crucial role. The density matrix is a complex $2[\ell] \times 2[\ell]$ hermitian matrix, this means that it has $4[\ell]^2$ independent elements. In order to analyze this fairly large matrix, we will decompose it into the most important and physical relevant terms. We will find that this decomposition largely simplifies the analysis, as well as it gives many new insights into the magnetism of the actinides, where the SOC plays a crucial role. The interaction term in Eq. (5.1) have been studied in detail, for example by Slater [52], Racah [53, 54, 55, 56] and Condon and Shortly [43]. By expanding the interaction in spherical harmonics and by making use of the Wigner-3j symbols [43] the interaction can be expressed as

$$\begin{aligned}\langle ab|g|cd\rangle =& \delta_{s_a s_c}\delta_{s_b s_d}[\ell]^2 \sum_{k=0}^{2\ell}\sum_{q=-k}^{k}(-1)^{m_a+m_b+q} \\ &\times \begin{pmatrix} \ell & k & \ell \\ 0 & 0 & 0 \end{pmatrix}^2 \begin{pmatrix} \ell & k & \ell \\ -m_a & -q & m_c \end{pmatrix} F^{(k)} \begin{pmatrix} \ell & k & \ell \\ -m_b & q & m_d \end{pmatrix}.\end{aligned} \tag{5.18}$$

The spin dependence is given by the two delta functions of the spin quantum numbers of states a, b, c and d. The radial dependence is confined in the Slater integrals $F^{(k)}$ and the Wigner-3j symbols take care of the angular part of the integral. We now introduce a multipole momentum tensor $\boldsymbol{w}^k$ defined as the

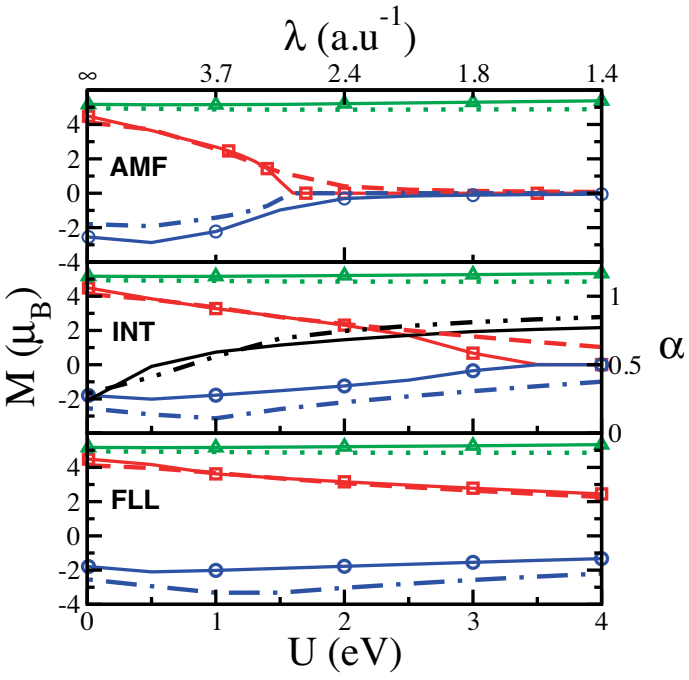

Figure 5.3: M_{sp} (red lines) and orbital M_{orb} (blue lines) magnetic moments of paramagnetic PuS (full line with squares for M_{sp}, full line with circles for M_{orb}), $a =$ 10.46 a.u., and ferromagnetic PuP (dashed line for M_{sp}, dashed-dotted line for M_{orb}), $a = 10.49$ a.u., as function of U for different types of DC. The Slater parameters are calculated SC by using a Yukawa potential with screening length λ reported in the upper axis. For AMF DC the moments vanish in both compounds at $U \approx 2.0$ eV, for FLL DC both compounds stay magnetic for all values of U. Only for the INT DC there is a range of U ($U \gtrsim 4.0$ eV) for which we obtain the experimental magnetic structure of both compounds [51]; PuS becomes non magnetic while PuP stays magnetic. The green lines refer to the $5f$ charge of PuS (full line with triangles) and PuP (dotted line). The black lines refer to INT DC factor α of PuS (full line) and PuP (dashed-two-dots line).

expectation values of a tensor operator $\boldsymbol{v}^k$,

$$w_x^k = \mathrm{Tr}\, v_x^k \rho \ , \tag{5.19}$$

$$v_x^k \equiv \left\langle m_b | v_x^k | m_a \right\rangle = (-1)^{\ell - m_b} \begin{pmatrix} \ell & k & \ell \\ -m_b & x & m_a \end{pmatrix} n_{\ell k}^{-1} \ , \tag{5.20}$$

$$n_{\ell k} = \frac{(2\ell)!}{\sqrt{(2\ell-k)!(2\ell+k+1)!}} \ . \tag{5.21}$$

If we view Eq. (5.19) as a transformation from ρ to $\boldsymbol{w}^k$, we can see that it is possible to invert it by utilizing an orthogonality property of 3j-symbols,

$$\sum_{kx} [k] \begin{pmatrix} \ell & k & \ell \\ -m_a & x & m_b \end{pmatrix} \begin{pmatrix} \ell & k & \ell \\ -m_c & x & m_d \end{pmatrix} = \delta(m_a, m_c)\delta(m_b, m_d) \, . \tag{5.22}$$

The inverse of Eq. (5.19) is then

$$\rho_{ab} = (-)^{m_b - \ell} \sum_{kx} [k] \begin{pmatrix} \ell & k & \ell \\ -m_b & x & m_a \end{pmatrix} n_{\ell k} w_x^k \, . \tag{5.23}$$

The spin independent part of the HF energy (the Hartree term) is defined as

$$E_{\mathrm{H}} = \frac{1}{2} \sum_{abcd} \rho_{ac} \left\langle ab | g | cd \right\rangle \rho_{bd} \ . \tag{5.24}$$

By now substituting in this expression Eq. (5.23) and Eq. (5.18) and by using the orthogonality relation

$$\begin{aligned} &\sum_{bd} (-)^{m_b + m_d} [k_1] \begin{pmatrix} \ell & k_1 & \ell \\ -m_d & x & m_b \end{pmatrix} \times \\ &\begin{pmatrix} \ell & k_2 & \ell \\ -m_b & q & m_d \end{pmatrix} = \delta(k_1, k_2)\delta(x, q) \ , \end{aligned} \tag{5.25}$$

we obtain a simple expression of the Hartree term in terms of tensor moments,

$$E_{\mathrm{H}} = \frac{[\ell]^2}{2} \sum_{k=0}^{2\ell} n_{\ell k}^2 \begin{pmatrix} \ell & k & \ell \\ 0 & 0 & 0 \end{pmatrix}^2 F^{(k)} \boldsymbol{w}^k \cdot \boldsymbol{w}^k \ , \tag{5.26}$$

where the scalar product is defined as

$$\boldsymbol{w}^k \cdot \boldsymbol{w}^k = \sum_{q=-k}^{k} w_q^k w_{-q}^k \ . \tag{5.27}$$

In order to take care of the spin dependence we may introduce a double tensor

$$w_{xy}^{kp} = \mathrm{Tr}\, v_x^k t_y^p \rho \tag{5.28}$$

$$t_y^p = (-1)^{s-s_b} \begin{pmatrix} s & p & s \\ -s_b & y & s_a \end{pmatrix} n_{sp}^{-1} \,. \tag{5.29}$$

It is easy to verify that $\boldsymbol{w}^{k0} = \boldsymbol{w}^k$. Again Eq. (5.28) can be inverted in a completely analogous way to Eq. (5.19),

$$\begin{aligned} \rho_{ac} = & \sum_{kx} [k] n_{lk} (-)^{m_c - \ell} \begin{pmatrix} \ell & k & \ell \\ -m_c & x & m_a \end{pmatrix} \sum_{py} [p] n_{sp} (-)^{s_c - s} \\ & \times \begin{pmatrix} s & p & s \\ -s_c & y & s_a \end{pmatrix} w_{xy}^{kp} \,. \end{aligned} \tag{5.30}$$

The transformations Eqs. (5.28) and (5.30) are one-to-one, as we can easily verify that the number of parameters are kept. The dimension of ρ is $2[\ell] \times 2[\ell]$ which gives $(4\ell+2)^2$ independent occupation numbers, since it is complex hermitian. The new occupation numbers are $\left[\sum_{k=0}^{2\ell}[k]\right] \times \left[\sum_{p=0}^{2s}[p]\right] = (4\ell + 1 + 1)(2\ell+1)/2 \times (4s+1+1)(2s+1)/2 = (4\ell+2)^2$, with $s = 1/2$. So we keep the same degrees of freedom, but now distributed on $[\ell][s]$ independent double tensors.

The exchange energy can also be written as function of the tensor components rather than the density matrix (see Appendix),

$$E_{\mathrm{X}} = -\sum_{2k=0}^{4\ell} F^{(k)} \sum_{k_1=0}^{2\ell} J(\ell,k,k_1) \sum_{p=0}^{1} \boldsymbol{w}^{k_1 p} \cdot \boldsymbol{w}^{k_1 p} \,, \tag{5.31}$$

where the interaction strength $J(\ell,k,k_1)$ is defined as

$$J(\ell,k,k_1) = \frac{1}{4}[\ell]^2 [k_1] (-)^{k_1} n_{\ell k_1}^2 \begin{pmatrix} \ell & k & \ell \\ 0 & 0 & 0 \end{pmatrix}^2 \begin{Bmatrix} \ell & \ell & k_1 \\ \ell & \ell & k \end{Bmatrix} . \tag{5.32}$$

Here the $\{...\}$ symbol is the Wigner $6j$-symbol. Notice that the $3j$-symbols are defined such that the contribution from odd k vanish, so only Slater parameters of even k are needed. This type of expression was derived by Racah [54]. However, since it was derived for atomic configurations only, it has not been fully realized that it is as valid for non-integer occupations.

5.5 The Coupling of Indices - Irreducible Spherical Tensor

It is convenient to introduce the irreducible spherical tensors $\boldsymbol{w}^{kpr}$ from the double tensors $\boldsymbol{w}^{kp}$ for two reasons. Firstly, the double tensors are not true spherical tensors and, secondly, in the presence of SOC the spin and orbital degrees of freedom are not longer decoupled. The three-index tensors $\boldsymbol{w}^{kpr}$ is defined through a coupling of the indices of the double tensor $\boldsymbol{w}^{kp}$,

$$w_t^{kpr} = \underline{n}_{kpr}^{-1} \sum_{xy} (-)^{k-x+p-y} \begin{pmatrix} k & r & p \\ -x & t & -y \end{pmatrix} w_{xy}^{kp} \,, \tag{5.33}$$

where the index r runs from $|k-p|$ to $|k+p|$, and where the normalization factor $\underline{n}_{abc}$ is given, as in Ref. [57], by

$$\underline{n}_{abc} = i^g \left[\frac{(g-2a)!(g-2b)!(g-2c)!}{(g+1)!} \right]^{1/2} \frac{g!!}{(g-2a)!!(g-2b)!!(g-2c)!!} \,, \tag{5.34}$$

with $g = a+b+c$. After having introduced the tensor w^{kpr} the transformations Eqs. (5.28) and (5.30) can be rewritten in a simplified matrix form,

$$\boldsymbol{w}^{kpr} = \mathrm{Tr} \boldsymbol{\Gamma}^{kpr} \boldsymbol{\rho} \,, \tag{5.35}$$

and

$$\boldsymbol{\rho}_{ab} = \sum_{kpr} \boldsymbol{\Lambda}_{ab}^{kpr} \cdot \boldsymbol{w}^{kpr} \,, \tag{5.36}$$

where the tensor matrices $\boldsymbol{\Gamma}$ and $\boldsymbol{\Lambda}$ are, respectively, defined as

$$\begin{aligned} \Gamma_{t,ab}^{kpr} =& N_{kpr\ell s}^{-1} (-)^{-m_a+\ell-s_a+s+k+p} \sum_{xy} (-)^{-x-y} \begin{pmatrix} \ell & k & \ell \\ -m_a & x & m_b \end{pmatrix} \times \\ & \begin{pmatrix} s & p & s \\ -s_a & y & s_b \end{pmatrix} \begin{pmatrix} k & r & p \\ -x & t & -y \end{pmatrix} \,, \end{aligned} \tag{5.37}$$

and

$$\begin{aligned} \Lambda_{t,ab}^{kpr} =& N_{kpr\ell s} [kpr] (-)^{m_b-\ell+s_b-s+r} \sum_{xy} \begin{pmatrix} \ell & k & \ell \\ -m_b & x & m_a \end{pmatrix} \times \\ & \begin{pmatrix} s & p & s \\ -s_b & y & s_a \end{pmatrix} \begin{pmatrix} k & r & p \\ x & t & y \end{pmatrix} \,. \end{aligned} \tag{5.38}$$

Here $N_{kpr\ell s} = \underline{n}_{kpr} n_{k\ell} n_{sp}$. The reversibility of the transformations is clear from the fact

$$\mathrm{Tr}\Gamma_t^{kpr}\Lambda_t^{k'p'r'} = (-1)^t \delta_{kk'}\delta_{pp'}\delta_{rr'}\delta_{tt'} \ . \tag{5.39}$$

The Hartree energy E_{H} of the shell ℓ in terms of the irreducible spherical tensor moments can be now written as

$$E_{\mathrm{H}} = \frac{[\ell]^2}{2} \sum_{k=0}^{2\ell} \sum_{r=-k}^{k} n_{\ell k}^2 \begin{pmatrix} \ell & k & \ell \\ 0 & 0 & 0 \end{pmatrix}^2 F^{(k)} \boldsymbol{w}^{k0r} \cdot \boldsymbol{w}^{k0r} . \tag{5.40}$$

The exchange energy E_{X} of the shell ℓ in terms of the irreducible spherical tensor moments is now

$$E_{\mathrm{X}} = -\sum_{2k=0}^{4\ell} F^{(k)} \sum_{k_1=0}^{2\ell} J(\ell,k,k_1) \sum_{p=0}^{1} \sum_{r} [r] (-)^{k_1+p+r} \underline{n}_{k_1 pr}^2 \boldsymbol{w}^{k_1 pr} \cdot \boldsymbol{w}^{k_1 pr} . \tag{5.41}$$

It is convenient to rewrite Eq. (5.41) in a simplified form,

$$E_{\mathrm{X}} = \sum_{k_1 pr} E_{\mathrm{X}}^{k_1 pr} = \sum_{k_1 pr} K_{k_1 pr} \boldsymbol{w}^{k_1 pr} \cdot \boldsymbol{w}^{k_1 pr} \ , \tag{5.42}$$

where

$$\begin{aligned} K_{k_1 pr} &= -\sum_{2k=0}^{4\ell} F^{(k)} J(\ell,k,k_1) [r] (-)^{k_1+p+r} \underline{n}_{k_1 pr}^2 \\ &= -\sum_{2k=0}^{4\ell} F^{(k)} \frac{[\ell]^2 [k_1][r]}{4} (-)^{k_1} |\underline{n}_{k_1 pr}|^2 n_{\ell k_1}^2 \\ &\quad \times \begin{pmatrix} \ell & k & \ell \\ 0 & 0 & 0 \end{pmatrix}^2 \begin{Bmatrix} \ell & \ell & k_1 \\ \ell & \ell & k \end{Bmatrix} . \end{aligned} \tag{5.43}$$

Here we substituted the interaction strength $J(\ell,k,k_1)$ defined in Eq. (5.32) and we used $(-)^{k_1+p+r} \underline{n}_{k_1 pr}^2 = |\underline{n}_{k_1 pr}|^2$. In Eq. (5.42) the exchange energy of the shell ℓ is expressed as a sum of independent terms involving different spherical tensors. We will refer to these terms as different exchange *channels*. In Fig 5.4 we plot an example of decomposition of the E_{X} in kpr-channels for US. In this case we identify three main contributions: the spin polarization (SP) term 011, the orbital polarization (OP) even term 110 and finally the high multipole of the magnetization, 615. These results are similar to ones we obtained in other uranium compounds that will be discussed in chapter 6.

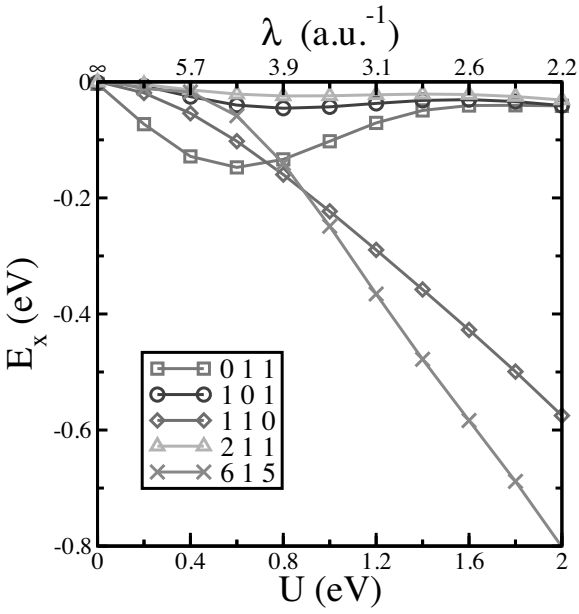

Figure 5.4: Relevant exchange energy channels $E_{\mathrm{X}}^{k_1 pr}$ in Eq. (5.42) of US calculated with LDA+U method and INT DC. The Slater parameters are calculated SC by using a screened Yukawa potential with screening length λ reported in the upper axis.

5.6 Physical Interpretation of Tensor Moments

The tensor moments can be related to a well-defined physical quantities, since they are proportional to the moment expansions of the charge (k even and $p = 0$), spin magnetization (k even and $p = 1$), current (k odd and $p = 0$) and spin current (k odd and $p = 1$) densities [58]. In table 5.1 we show some examples. The time reversal parity of $\boldsymbol{w}^{kpr}$ is given by $(-1)^{k+p}$. Hence $\boldsymbol{w}^{101}$ is also referred to as odd OP, since it breaks the time-reversal symmetry, while $\boldsymbol{w}^{110}$ does not and, consequently, it is referred as OP-even polarization and it is thus compatible with a non magnetic solution, as clarified in paper IV.

5.7 Polarization Channels

The exchange energy channels are not completely independent, since the spherical tensors have to describe a physical density matrix ρ. Then there is a restriction that the density matrix needs to have positive eigenvalues between zero and one, or equivalently

$$\mathrm{Tr}\,\rho \geq \mathrm{Tr}\,\rho^2\,. \tag{5.44}$$

Table 5.1: *Relation between some tensor operators $\boldsymbol{w}^{kpr}$ and standard ground state operators [58].*

	w_t^{kpr}	ℓ-shell
Number operator	w_0^{000}	n_ℓ
Isotropic SO coupling	w_0^{110}	$(\ell s)^{-1}\sum_i \boldsymbol{l}_i \cdot \boldsymbol{s}_i$
Anisotropic SO coupling	w_0^{112}	$3\ell^{-1}\sum_i (l_z s_z - \frac{1}{3}\boldsymbol{l}\cdot\boldsymbol{s})_i$
Orbital moment	w_0^{101}	$-\ell^{-1}\sum_i l_{z,i}$
Spin moment	w_0^{011}	$-s^{-1}\sum_i s_{z,i}$
Charge quadrupole moment	w_0^{202}	$3[\ell(2\ell-1)]^{-1}\sum_i (l_z^2 - \frac{1}{3}\boldsymbol{l}^2)_i$
Magnetic dipole moment	w_0^{211}	$-(2\ell+3)\ell^{-1}T_z$

When the tensors take as large values as this restriction allows, we say that the corresponding channel is saturated. A completely unpolarized density matrix is proportional to the identity matrix, it corresponds to that all spherical tensors are zero except for $\boldsymbol{w}^{00}$. That makes it natural to talk about polarization channels, when the spherical tensors acquire non-zero magnitudes. When the density matrix has integer eigenvalues, i.e. zero or one, we refer to it as fully polarized or localized. Only in this limit we have the equality in Eq. (5.44). In order to study general polarizations, we will expand the terms in Eq. (5.44) in spherical tensors.

By using the representation of the density matrix in Eq. (5.30), the properties of the Wigner-3j symbols and the fact that $\boldsymbol{w}^{00} = \mathrm{Tr}\,\rho$, we rewrite Eq. (5.44) in terms of double tensor moments

$$\boldsymbol{w}^{00} \geq \sum_{kp} [k][p] n_{\ell k}^2 n_{sp}^2 \boldsymbol{w}^{kp} \cdot \boldsymbol{w}^{kp} \,. \tag{5.45}$$

Let us now rewrite Eq. (5.45) in terms of the irreducible spherical tensor $\boldsymbol{w}^{kpr}$, as defined in Eq. (5.33)

$$\boldsymbol{w}^{000} \geq \sum_{kpr} [k][p][r](-)^{k_1+p+r} N_{kpr\ell s}^2 \boldsymbol{w}^{kpr} \cdot \boldsymbol{w}^{kpr} = \sum_{kpr} \frac{[k][r]}{2} |\underline{n}_{kpr}|^2 n_{lk}^2 \boldsymbol{w}^{kpr} \cdot \boldsymbol{w}^{kpr} \,, \tag{5.46}$$

since $[p] n_{sp} = 1/2$ for $s = 1/2$ and $p = 0, 1$. We now subtract the 000 term from the sum on the RHS and, by considering that $\boldsymbol{w}^{000} = \mathrm{Tr}\,\rho = n$, with n number of occupied electrons, that $n_{\ell 0}^2 = [\ell]^{-1}$ and that $\underline{n}_{000}^2$=1, we obtain

$$\boldsymbol{w}^{000} \geq \frac{1}{2[\ell]} \boldsymbol{w}^{000} \cdot \boldsymbol{w}^{000} + \sum_{kpr \neq 000} \frac{[k][r]}{2} |\underline{n}_{kpr}|^2 n_{\ell k}^2 \, \boldsymbol{w}^{kpr} \cdot \boldsymbol{w}^{kpr} \,. \tag{5.47}$$

Multiplying both sides by $2[\ell]$ and rearranging the terms, we obtain

$$n(2[\ell]-n) = nn_h \geq \sum_{kpr\neq 000} [\ell][k][r]|\underline{n}_{kpr}|^2 n_{\ell k}^2 \boldsymbol{w}^{kpr}\cdot\boldsymbol{w}^{kpr} = \sum_{kpr\neq 000} c^{kpr}\ , \tag{5.48}$$

where n_h is the number of holes and c^{kpr} refers to the polarization of channel kpr. Now the equality corresponds to a fully polarized system, while the unpolarized case has a vanishing RHS. In the case of itinerant systems the sum of polarizations is always smaller than nn_h since the system is not localized but only partially polarized. The corresponding exchange energy that is gained by polarizing these channels can be obtained from Eq. (5.41),

$$E_{\rm X} = \sum_{kpr} E_{\rm X}^{kpr} = -\sum_{kpr} A_{kpr} c^{kpr}\ , \tag{5.49}$$

where

$$A_{kpr} = \sum_{2n=0}^{4\ell} \frac{[\ell]}{4} \begin{pmatrix} \ell & n & \ell \\ 0 & 0 & 0 \end{pmatrix}^2 \begin{Bmatrix} \ell & \ell & k \\ \ell & \ell & n \end{Bmatrix} F^{(n)}\,. \tag{5.50}$$

One of the most relevant types of polarization is the so-called spin polarization (SP), often referred to as Stoner exchange or Hund's first rule, which corresponds to a polarization of channel 011. Since $c^{011} = m_{\rm spin}^2$, we get that the SP energy $E_{\rm SP}$ is given by,

$$E_{\rm SP} = -A_{011} m_{\rm spin}^2 = -\frac{1}{4}\left(\frac{U-J}{2\ell+1}+J\right) m_{\rm spin}^2\ . \tag{5.51}$$

The so-called Stoner parameter I, defined by $E_{SP} = -\frac{1}{4} I m_{\rm spin}^2$, is given by

$$I = \frac{U-J}{2\ell+1} + J\ , \tag{5.52}$$

as it is well known [12]. In this expressions we have adopted the convention to use the "Hubbard"-parameters, that are a linear combination of Slater parameters. For d and f electrons $U = F^{(0)}$ and J is expressed respectively as

$$J^d = \frac{1}{14}(F^{(2)} + F^{(4)})\ , \tag{5.53}$$

$$J^f = \frac{2F^{(2)}}{45} + \frac{F^{(4)}}{33} + \frac{50F^{(6)}}{1287}\ . \tag{5.54}$$

In Fig. 5.5 we compare for US the relative SP 011, with the polarization of 615-channel, that corresponds to an high multipole of the magnetization. It is interesting to note that while 011 component is decreasing with increasing U, the 615 component rapidly increases. In our multipole expansion in

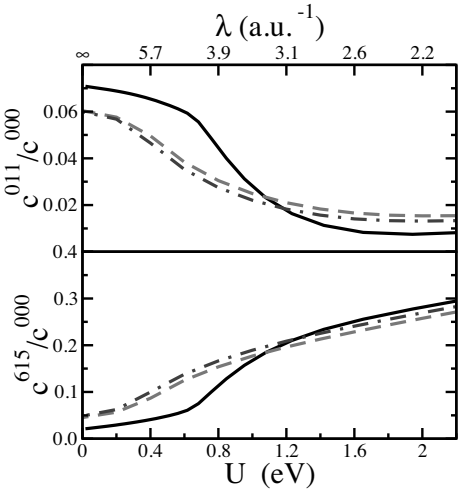

Figure 5.5: Relative polarization of 011 (upper panel) and 615 (lower panel) components of tensor moment in US ($a = 10.36$ a.u.) calculated with LDA+U approach. We compare the results obtained by calculating the $F^{(k)}$s with a screened Yukawa potential (black line, screening length in the upper axis) with ones obtained by fixing the ratios A_1 and A_2 to ones of Ref. [47, 9] (red dashed line) and to ones of Ref. [45, 46] (blue dashed-dotted line). In the calculations with fixed ratios the parameter J has been set to 0.46 eV [45].

Eq. (5.42) it is also included an exact formulation of the orbital polarization (OP) exchange energy $E_{\rm OP}$,

$$E_{\rm OP} = E_X^{101} + E_X^{110} = K_{101}\boldsymbol{w}^{101}\cdot\boldsymbol{w}^{101} + K_{110}\boldsymbol{w}^{110}\cdot\boldsymbol{w}^{110}\,, \tag{5.55}$$

where $K_{101} = 3K_{110}$ and $\boldsymbol{w}^{101}\cdot\boldsymbol{w}^{101} = m_{\rm orb}^2/\ell^2$. This expression is a sum of two terms, the OP-odd 101 term and the OP-even 110 term. Finally the prefactor K_{101} has a simple expression in terms of Racah parameters [47]. For d and for f electrons K_{101} is expressed respectively as

$$K_{101}^d = -\frac{E^0 + 21E^2}{10}\,, \tag{5.56}$$

$$K_{101}^f = -\frac{9E^0 + 297E^3}{112}\,. \tag{5.57}$$

6. Analysis of Results and Discussion

In this chapter we shall apply the methods described in the previous sections to different actinide and Fe-pnictide compounds and discuss the results. In section 6.1 we will main focus on the explanation of the non-magnetic phase of δ-Pu (see papers IV and IX). In section 6.2 we will show results for uranium compounds with their large triakontadipole exchange energy channel (see papers II, III and VIII). Then in section 6.3 we will provide argumentations that this large multipole of the magnetization density constitutes the HO parameter in the heavy-fermion superconductor URu_2Si_2 (see paper III). In sections 6.4 and 6.5, we will underline the central role played by the triakontadipole moments in hexagonal actinide superconductors (paper V) and in the actinide dioxide insulators (paper VII), respectively. In section 6.6 we will discuss how these results lead to a formulation of a new set of rules, the Katt's rules, that are valid for itinerant systems in case of large spin-orbit coupling (SOC), instead of those of Hund (see paper VIII). Finally, in section 6.7 we show that for the ferro-pnictides, a new class of high-T_C superconductors, a low-spin moment solution is stabilized over a large moment solution, due to the gain in exchange energy in the formation of large multipoles of the spin magnetization density (see paper VI).

6.1 Enhancement of Orbital Spin Currents in δ-Pu

In the recent years there have been many attempts to understand the phase diagram of Pu, especially the formation of its high-temperature and large volume δ-phase. It was observed that the experimental volume of this phase could be reproduced in spin-polarized calculations [59, 60]. However the prediction of any magnetic moment contradicts a large number of experiments [61]. Recently it was found that a non-magnetic phase with the correct experimental volume could be obtained by utilizing the LDA+U approach, with inclusion of the off-diagonal spin terms in the density matrix [44]. This is a counter-intuitive finding, since the moment of δ-Pu vanishes by increasing the exchange energy. In this work we applied the multipole decomposition of the screened Hartree-Fock (HF) exchange energy in order to understand how the non-magnetic state is stabilized by the LDA+U approach, as described in paper IV. In Fig. 6.1 we show the moments and exchange energy channels E_{X}^{kpr}, Eq. (5.42), from LDA+U

calculations of Pu with AMF type of double-counting (DC). Starting from the magnetic LDA solution with large moments, spin and orbital moments vanish already for $U = 0.8$ eV (J=0.68 eV). At the same time, in the exchange energy the spin polarization (SP) channel 011 is taken over by the orbital polarization (OP) even channel 110. The OP-odd term 101, related to the presence of an orbital moment, is barely detectable for low U, and it also completely vanishes once the 110 channel takes over. We would like to stress that although there is a small increase in the $5f$ occupancy from 5.2-5.5 electrons, it has little influence, in contrast to what has been assumed in other studies [44, 62]. It is clear from Fig. 6.1 that it is the increase of $\boldsymbol{w}^{110}$, and its corresponding energy channel, that stabilizes a non-magnetic solution. As explained in chapter 5, the time-reversal-even order parameter $\boldsymbol{w}^{110}$ arises from spin currents and it is proportional to the spin-orbit-like operator $\boldsymbol{l} \cdot \boldsymbol{s}$. It corresponds to the situation in which the three components of the spin current orbit with same magnitude around their respective quantization axis. Recently there have been indirect measurements of the magnitude of $\boldsymbol{w}^{110}$ for several actinides [63, 64] by using a sum rule [65] applied to the branching ratios from d to f transition. These studies report very large values, not least for α-Pu and they attribute this to the strong SOC bringing the $5f$ states close to a jj coupling limit. In this work we would like to change this analysis. While the SOC is important in the actinides, it is not strong enough to bring by itself the $5f$ in the jj scheme. In fact without the screened HF term in Eq. (5.1) we calculated $\boldsymbol{w}^{110}$ to be equal to -2.3. While in the presence of the HF term $\boldsymbol{w}^{110}$ gets enhanced values between -4.4 and -7.2. These values have to be compared with the measured value of -5.1 for α-Pu, assuming a f^5 configuration [65]. The exchange term is then essential to bring the theoretical $\boldsymbol{w}^{110}$ to the same magnitude of the experimental value, i.e. to give rise to enhanced values of the orbital spin currents, $\boldsymbol{w}^{110}$, obtained in recent experiments [63, 64]. This finding is also confirmed by a DMFT study presented in paper IX.

In Fig. 6.2 we plot the magnitude of $\boldsymbol{w}^{110}$ for other elements of the actinide series by obtaining a good agreement with the measured ones [3]. The largest $\boldsymbol{w}^{110}$ is obtained for non-magnetic Pu and Am, with a value very close to saturation. Cm shows a much smaller value, in according with the pronounced shift in the coupling mechanism of $5f$ states toward a more LS-like behaviour [3, 66].

The determination of the equilibrium volume in δ-Pu turned out to be very sensitive to the choice of the linearization energies of the APWs and of the local orbitals. If these energies are wisely chosen in the correct energy region corresponding to $j = 5/2$ states, we obtain a very good agreement with the experimental equilibrium volume, as we illustrate in Tab. 6.1 and in Fig. 6.3.

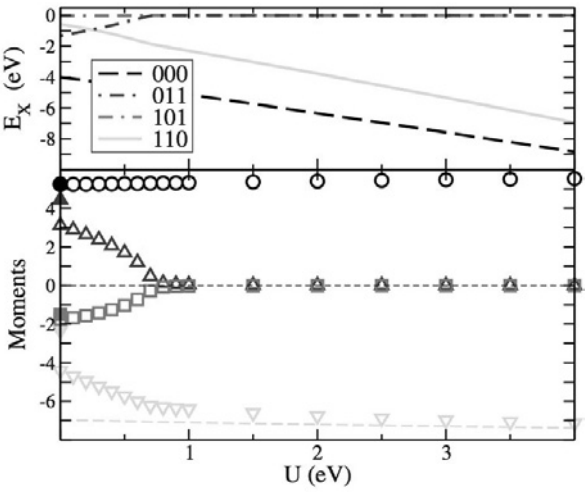

Figure 6.1: Moments and exchange energies from LDA+U-AMF calculations of fcc Pu ($a = 8.76$ a.u) within the FP-APW+lo method. The spin (up-pointing triangles) and orbital (squares) moments are shown in the bottom part for a varying U but a constant $J = 0.68$ eV. Filled symbols indicate the LDA results. Also displayed is the $5f$ occupation number (circles) as well as $\boldsymbol{w}^{110}$ (down-pointing triangles) where the dashed line indicates the corresponding saturation limit $-\frac{4}{3}w_0^{000}$. At the top, the most significant channels of the exchange energy , E_X^{kpr}, are displayed as lines, with same notational scheme as for the moments, with the tensor rank identifying each, given in the legend.

Table 6.1: *Comparison of theoretical and experimental equilibrium volume V_0 and bulk modulus B_0 of δ-Pu. In our calculations the linearization energies of f-APW+*lo *are chosen equal to $3/4$ of the Fermi energy in order to accurately describe the $j = 5/2$ states. We determined the Slater integrals individually through a Yukawa potential with screening length corresponding to U=4 eV. Fo this U we obtained vanishing moments both in AMF and in INT LDA+U at all volumes in the range 140-210 a.u.*[3]*. For INT type of DC, the interpolation constant α is fixed to the one obtained at the experimental volume.*

	Method	V_0 [a.u.[3]]	B_0 [GPa]
This work	AMF LDA+U	169	462
This work	INT LDA+U (α=0.8)	174	552
Shick et al. [44]	AMF LDA+U	181.5	314
Ledbetter et al. [68]	Expt.	168	299

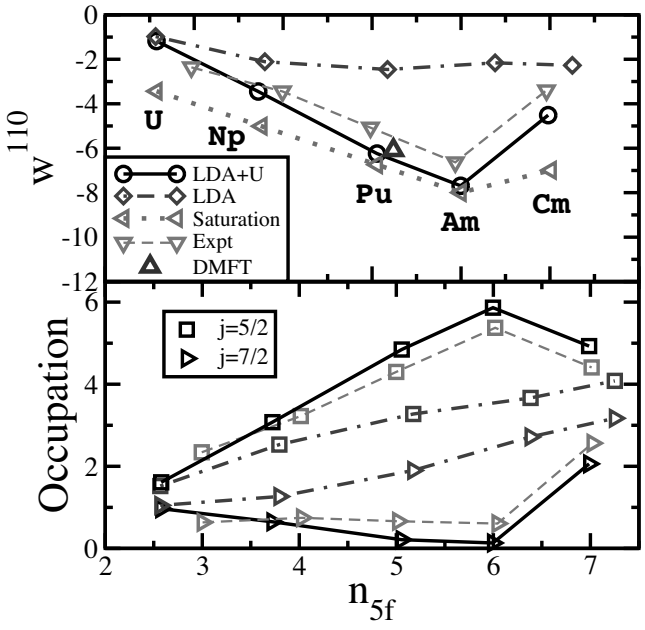

Figure 6.2: Top panel: ground-state SOC interaction $\boldsymbol{w}^{110}$ in actinides as functionof the number of $5f$ electrons n_{5f}. Theoretical LDA, LDA+U and DMFT values are from this study [67]. The saturation value refers to LDA+U results [67]. The experimental points refer to the spin-orbit sum-rule analysis of the measured branching ratios of each metal [3]. Bottom panel: electron occupation of $j = 5/2$ and $j = 7/2$ levels as unpolarized n_{5f}. The color-line scheme is the same as in the top panel, while the symbols refer to j as indicated in the legend. The experimental points are obtained through the spin-orbital analysis of the EELS spectra [3].

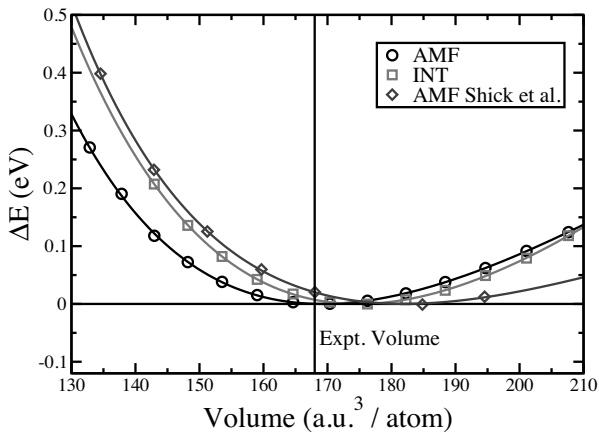

Figure 6.3: Comparison between LDA+U energy-volume curve of δ-Pu, obtained in this work with both AMF and INT DC, and the LDA+U-AMF curve of Shick et al. [44].

6.2 Triakontadipoles in Uranium Magnetic Compounds

In this study we apply the LDA+U method and its multipole decomposition to a few different magnetic uranium systems (see papers II, III and VIII); three supposedly normal systems; UAs, US and USb in the NaCl-structure, and URu_2Si_2 with its enigmatic HO in the tetragonal $ThCr_2Si_2$ structure. We display the calculated magnetic moments in Fig. 6.4 as unpolarized the parameter U. We observe that we have a good agreement with the experimental moments [69] for U in the range 0.6-1.0 eV, which is the range of reasonable values for the $5f$ states of uranium. The magnetic moments are also of the same magnitude of other studies that go beyond LDA [49, 70]. The calculated spin and orbital moments (M_{sp} and M_{orb}) present slightly different behaviour for the different compounds. For UAs M_{orb} increases with U in a monotonous way and M_{sp} is constant, while, for US and USb, M_{orb} reaches a maximum value around 0.6 eV and M_{sp} decreases in a monotonous way. The last behaviour is again counter-intuitive as in case of δ-Pu; M_{sp} decreases by increasing the exchange energy. To better understand this fact we decompose the exchange energy in tensor moment contributions E_{X}^{kpr} in Fig. 6.4. Like in δ-Pu we observe that the SOC-like multipole $\boldsymbol{w}^{110}$ has a large contribution to the total exchange energy. However, the most surprising effect is that a non-trivial high multipole of the magnetization density, the tensor $\boldsymbol{w}^{615}$, becomes very large. More specifically, we can observe that, with increasing U, the 615 contributions completely dominates the exchange energy when the SP term 011 decreases to small values. This trend is particular clear in case of URu_2Si_2, whose spin moment crosses zero at $U \approx 1.25$ eV. In Figs. 6.5 and 6.6 we plot the shape of the magnetization density $\boldsymbol{m}^{615}(\boldsymbol{r})$ associated with $\boldsymbol{w}^{615}$. We can observe that $\boldsymbol{m}^{615}(\boldsymbol{r})$ is highly non-collinear: it is closely related to the intra-atomic non-collinear spin density that always arise in the presence of SOC [71]. Since the exchange coupling enhances substantially the effective SOC, the resulting 615-polarization becomes more important than the ordinary SP. For all cases, except UAs, the 615 contribution to the exchange energy bypasses the one of SP 011 for values of U around 1 eV. A large 615 term is also detected in few Np compounds, for example in NpN, while in Pu magnetic compounds, like PuP, the calculated 615 contribution is much smaller. A systematic explanation of this trend is given in section 6.6 and in Fig. 6.13.

6.3 Triakontadipoles Moments as the Hidden Order in URu_2Si_2

The nature of the hidden order (HO) parameter in URu_2Si_2 is still an unsolved mystery. At 17.5 K this compound undergoes a second-order phase

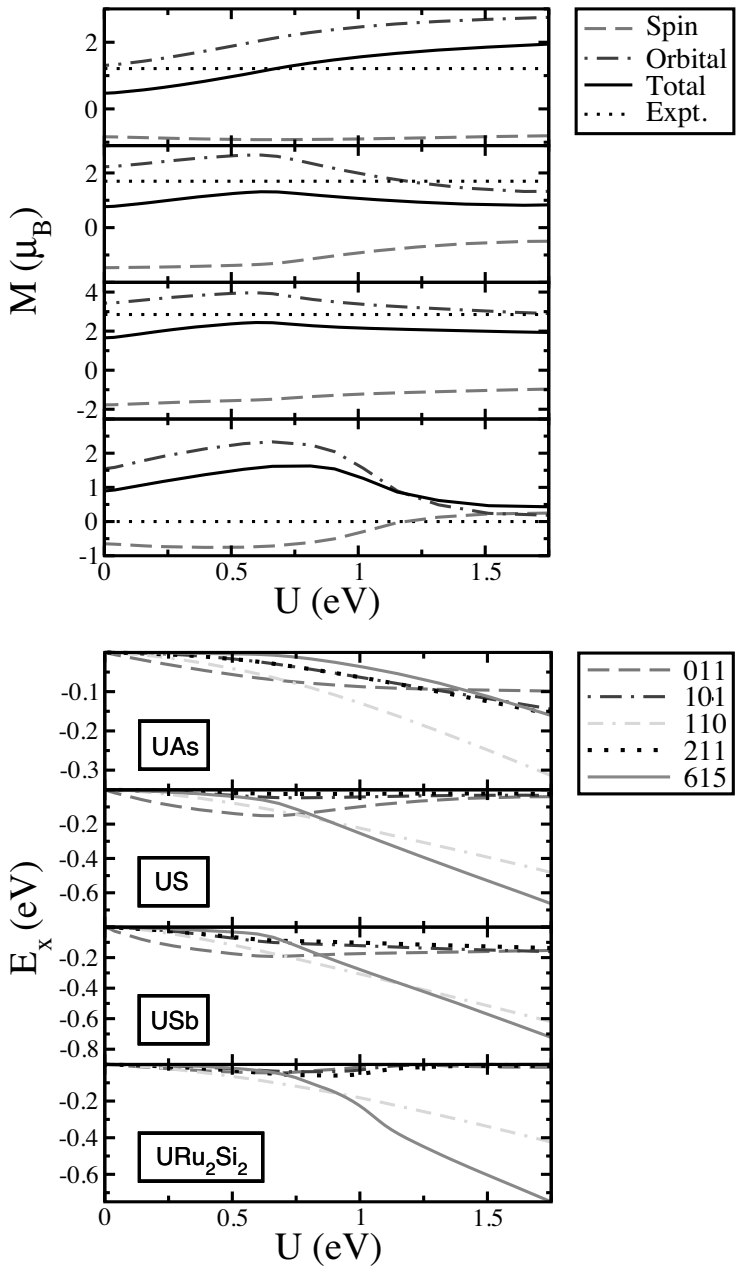

Figure 6.4: Top panel: the calculated spin (red dashed line), orbital (blue dashed-dotted line) and total (full black line) magnetic $5f$ moments as unpolarized U, for various magnetic uranium compounds (whose labels are located in the bottom panel). The case $U = 0$ corresponds to the LDA-limit. The experimental magnetic moment is given by the black dotted line. Bottom panel: the contributions to exchange energy from the relevant *kpr* channels in Eq. 5.42 as functionof U.

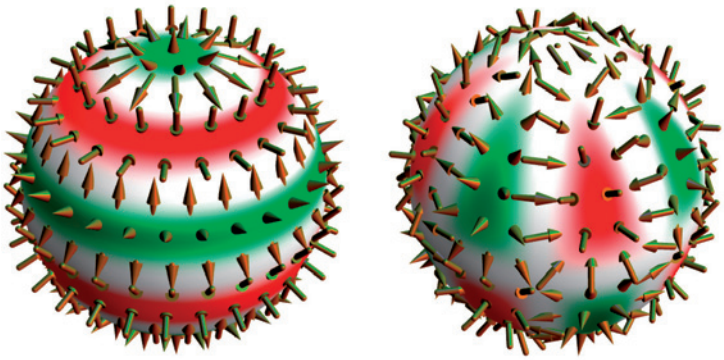

Figure 6.5: The angular variation of the direction of the spin density for the two non-vanishing components of the triakontadipole in URu_2Si_2, w_0^{615} and $w_{\pm4}^{615}$ in tesseral form [72]. The green (red) colour indicates the regions where the spin axis is outward (inward) normal.

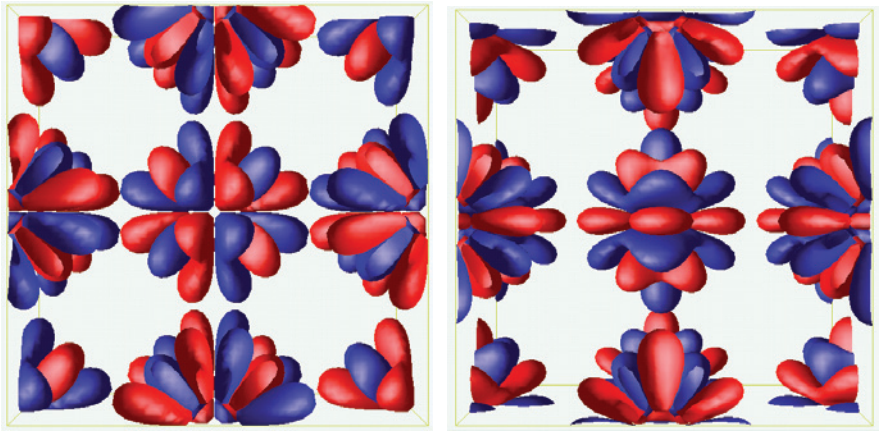

Figure 6.6: Isosurfaces of the x-component (left panel) and z-component (right panel) of the magnetization density arising from the 615-multipole in antiferromagnetic 1-$\boldsymbol{k}$ structure of UAs with spin quantization axis along [001], which is upwards in the figure. The red and negative lobes correspond, respectively, to positive and negative isosurfaces of magnitude 0.005 $\mu_B/\text{a.u.}^3$.

transition that shows a sharp variation of bulk properties, in particular specific heat [73], linear and non-linear susceptibilities [73, 74, 75, 76], resistivity [77] and thermal expansion [78]. The exponential dependence of the specific heat [78] and the gap in magnetic excitation spectra [79, 80] clearly indicate a magnetic transition, however the size of the observed moment is very small (0.03 μ_B) [81]. Many theories, more or less exotic, have been proposed to explain the HO in this material. Some of these explanations are of localized nature e.g. quadrupoles [82] or octupoles [83], and some of itinerant nature as e.g. spin nematics [84], orbital currents [85], helicity order [86], or fluctuating moments [87]; but none of them have been consistent with all experimental observation in a satisfactory way. In this study, as illustrated in paper III, we find that the non-trivial magnetic triakontadipole moments, associated with the tensor moments $\boldsymbol{w}^{615}$, constitute the HO parameter in URu_2Si_2. Our calculations, which treat the $5f$ states as itinerant with large Coulomb interaction, show that what makes URu_2Si_2 unique is the very large triakontadipole moment which forces both spin and orbital dipole moments to vanish. In Fig. 6.4 we observe two striking differences compared to other uranium compounds. Firstly, the polarization of the 615-channels is even more prominent and, secondly, at large U (1.2 eV) the M_{sp} switches sign and becomes parallel to the M_{orb} and both moments become very small. These properties signal some anomaly, and we proceed to study this phase under pressure. From careful analysis of the results of experiments under uni-axial stress, one can conclude that the main variation in the pressure experiments arises from the contraction of the tetragonal a-axis [88]. Therefore we perform calculations with varying lattice constant a, to mimic the effect of pressure. The results for $U = 0.9$ eV are shown in Fig. 6.7, where we see a dramatic effect on the magnetic moments from small variations in lattice constant a away from a critical value, slightly larger (1.4 %) than the experimental value a_0. At this critical value both M_{sp} and M_{orb} vanish, while simultaneously the 615 contribution to the exchange energy almost diverges. In fact all the vector contributions, 011, 101 and 211, go to zero at this point.

Can the 615-tensor order parameter be observed at this critical lattice point where dipole tensors vanish? Due to its high rank it is indeed a well hidden order parameter, but since there is a magnetization density associated with it, as in Figs. 6.5 and 6.6, it will give rise to magnetic scattering in e.g. neutron diffraction experiments although the integrated moment is zero. One problem though is that it belongs to the same point group representation as any non-vanishing dipole order [11], so very careful analysis on high accuracy experiments is needed to distinguish this pure HO case from a tiny dipole moment case.

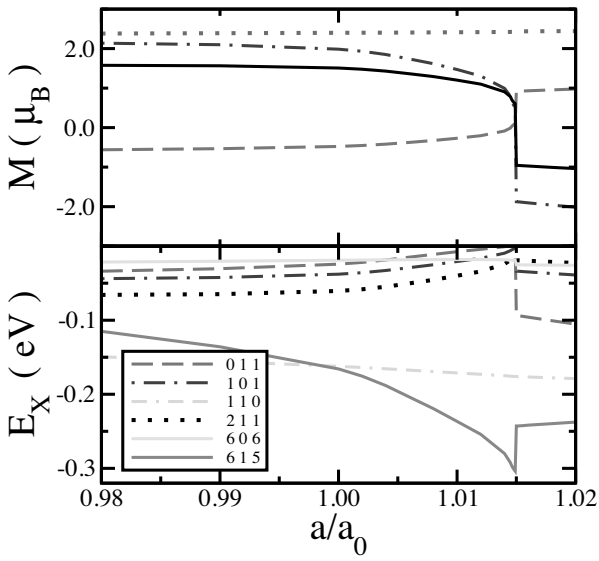

Figure 6.7: Upper panel: the spin, orbital and total magnetic moments in URu_2Si_2 (same color scheme as Fig. 6.4), are shown as functionof variation in the in-plane lattice constant a with respect to the experimental one a_0, calculated with $U = 0.9$ eV. The $5f$ occupation is represented by a green dotted line. Lower panel: the non-vanishing contributions to the exchange energy, E_{X}^{kpr}, as unpolarized a.

6.4 Triakontadipoles in Hexagonal Actinide Superconductors

As presented in paper V, we investigate the ground state of the heavy-fermion actinide compounds UPd_2Al_3, UNi_2Al_3 and UPt_3 by means of electronic structure calculations including on-site correlation. In case of UPd_2Al_3 and UNi_2Al_3, we stabilize a solution with an antiferromagnetic arrangement of triakontadipoles with ordering vectors, respectively, $\boldsymbol{q} = (0,0,\frac{1}{2})$ and $\boldsymbol{q} = (\frac{1}{2},0,\frac{1}{2})$, whose total magnetic moment agrees with the experimental value [89, 90]. In case of UPt_3 we identify a solution with a triakontadipole order whose symmetry is not compatible with the presence of a magnetic moment, in accordance with experiments that detect a very small value of the moment [91]. The Fermi surfaces of the multipole-dominated solutions have many common features with those obtained by conventional density functional methods [92, 93]. Finally, for URu_2Si_2 we are able to stabilize a new solution characterized by a $\boldsymbol{q} = (0,0,\frac{1}{2})$ ordering of triakontadipoles and a symmetry that forbids a magnetic moment on uranium sites. The Fermi surface of this solution is surprisingly similar to the one of the magnetic AF 1-$\boldsymbol{q}$ case, in agreement with recent measurements [94].

6.5 Multipolar Magnetic Ordering in Actinide Dioxides

As illustrated in paper VII, the LDA+U method and its multipole decomposition are applied to investigate the ground state of the actinide dioxide insulators UO_2, NpO_2 and PuO_2. In case of UO_2, an antiferromagnetic 3-$\boldsymbol{k}$ type ordering of U moments is identified as one of the lowest energy solutions, in agreement with experiments [95] and recent calculations [96]. For NpO_2, a magnetic multipolar 3-$\boldsymbol{k}$ ordering of triakontadipoles, with a zero net magnetic moment on Np atoms, is found to be one of the most stable solutions. This is in agreement with recent investigations that predict the triakontadipoles to be the hidden order parameter in NpO_2 [97]. Also in case of the non-magnetic insulator PuO_2, the ground-state is predicted to be described by a multipolar 1-$\boldsymbol{k}$ ordering of triakontadipoles associated with a magnetization density that integrates to zero on Pu sites.

6.6 Time Reversal Symmetry Breaking in Itinerant Systems

Spontaneous polarization of the density matrix is related to symmetry breaking. For atoms in a crystal some polarizations of charge multipoles are always present due to directional bonds. The presence of a spontaneous polarization in the system is the result of a subtle competition between gain in exchange energy and loss of kinetic energy. In case of itinerant systems the most important symmetry breaking is the one of time-reversal (TR) symmetry. In its presence all electronic states are doubly degenerate. This corresponds to a spin degeneracy in absence of SOC. However, in presence of finite SOC interaction the degeneracy is more complicate with a mixed character of both spin states.

6.6.1 Hund's Rules

In the limit of weak SOC the TR symmetry is effectively broken by the SP. In the tensor moment formalism this corresponds to a polarization of the channel 011. The saturation of 011 channel, or Hund's first rule, corresponds to a density matrix with this form,

$$\rho = \frac{n}{[\ell]}\mathrm{diag}\{1_{[\ell]}, 0\} \,, \tag{6.1}$$

for $n < [\ell]$, with n number of electrons and $[\ell] = 2\ell + 1$. Hund's second rule then corresponds to saturate the 101 channel, by maximizing the orbital moment. This is the OP-odd channel [7]. Hund's second rule arises from atomic physics, where it was observed that the terms with maximum L, or equivalently orbital moment, were lowest in energy if the system was fully spin

polarized. However, this is true for localized systems where we have full polarization, i.e. where many channels contribute to a maximum polarization. In this study we are more interested in itinerant systems, for which the density matrix is not idempotent, i.e. the equality in Eq. (5.44) is not fulfilled and, consequently, only a few exchange channels polarize. However, for a fully spin polarized system, the 101-channel cannot polarize by itself since that would give arise to a non-physical density matrix, i.e. one that breaks the condition of Eq. (5.44). Instead a straight-forward analysis gives that a combined polarization of 101, 110 and 112 gives rise to an optimal orbital moment slightly smaller than that of a localized fully polarized system. This combination of fully polarized spin moments and optimally polarized orbital moments, more relevant for itinerant solid state systems, will be called modified Hund's rules. These polarizations are summarized in Fig. 6.8, where the SP 011 and OP-odd 101 are given separately. We observe that especially for low occupation numbers we are far below the fully polarized limit. In the case of half-filled shell, however, the SP corresponds to the localized, fully polarized limit. In the actinide compounds we consider in this work, Hund's rules are far away from fulfilled, since the SP does not play the dominant role as always assumed. In Figs. 6.9 and 6.10 we present the polarizations of the density matrices for LDA calculations ($U = 0$) and those for LDA+U calculations, respectively. They summarize quite well the main observation of this study. On one hand the LDA calculations show large SP which leads to an overestimation of the spin moments. At the other hand, when including the extra interactions of the LDA+U calculations, the total polarization increases but, more importantly, another polarization channel dominates, the one of spin-orbital currents, the OP-even 110 channel. This channel is even close to saturation for all systems. This corresponds to a large enhancement of SOC interaction in all these compounds. The SP 011, however, decreases drastically, and in some Pu compounds even disappears. The only exception is Cm where the SP 011 dominates over the OP-even 110, in accordance with the expected *LS*-coupling mechanism of $5f$ electrons in this material [3]. As already mentioned, to some surprise, a third polarization plays a larger role, the 615-channel. These results have influenced to formulate a set of new rules to be valid in the case of stronger SOC, instead of those of Hund, as shown in paper VIII.

6.6.2 Katt's Rules

In the non-relativistic limit it is the double degeneracy in the spin degrees of freedom, which is so simple to break, that makes Hund's first rule so effective. In the actinide case, with the fairly strong SOC interaction, this simple spin degeneracy does not exist in the un-polarized case. In the presence of SOC our analysis arrives at an alternative set of rules, which we will denote as Katt's rules (see paper VIII). These rules are summarized in Fig. 6.13. Firstly, the

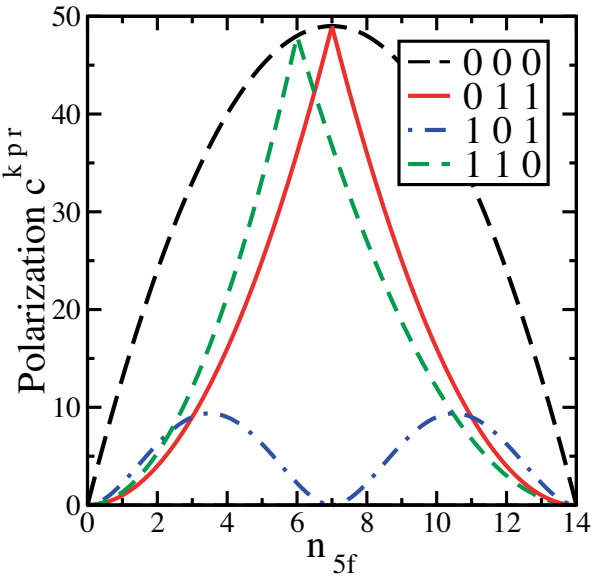

Figure 6.8: Saturation values of polarization c^{kpr}, as defined in Eq. (5.49) of different tensor moments assuming full localization: 000 (black line), 011 (red line), 101 (blue line, assuming Hund's first rule fulfilled) and 110 (green line).The latter value is obtained from the saturation value of $\boldsymbol{w}^{110}$ equal to $-\frac{4}{3}n_{5/2}+n_{7/2}$, where $n_{5/2}$ and $n_{7/2}$ indicate, respectively, the occupation of $j=5/2$ and $j=7/2$ states.

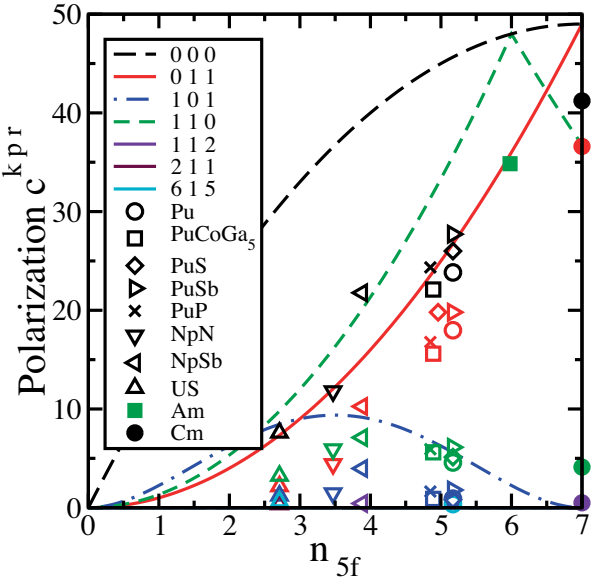

Figure 6.9: The polarization of the density matrix c^{kpr} resulting from a LDA calculation ($U=0$ eV) for the compounds considered in this study. The full curves have the same meaning as in Fig. 6.8.

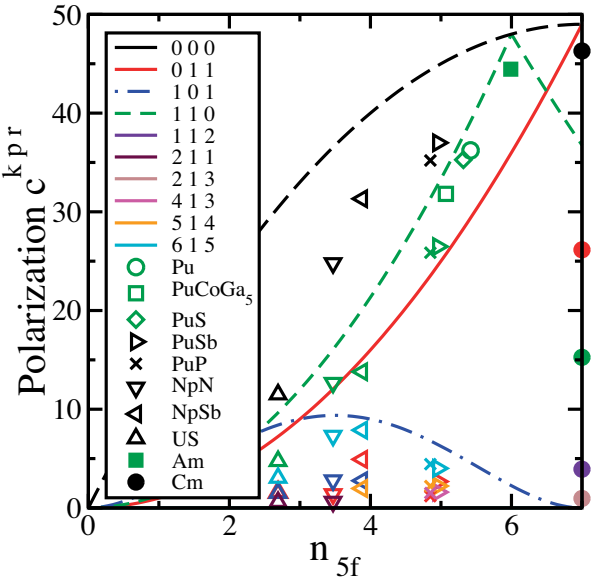

Figure 6.10: The polarization of the density matrix c^{kpr} resulting from LDA+U calculations for U, Np and Pu compounds. For the U, Np and Pu systems we have used U equal to 0.75, 2.5 and 4.0 eV, respectively. For Am and Cm we have used $U = 4.0$ eV and $U = 5.0$ eV, respectively. Note that for the non-magnetic Pu systems the total and 110-polarization coincide. The full curves have the same meaning as in Fig. 6.8.

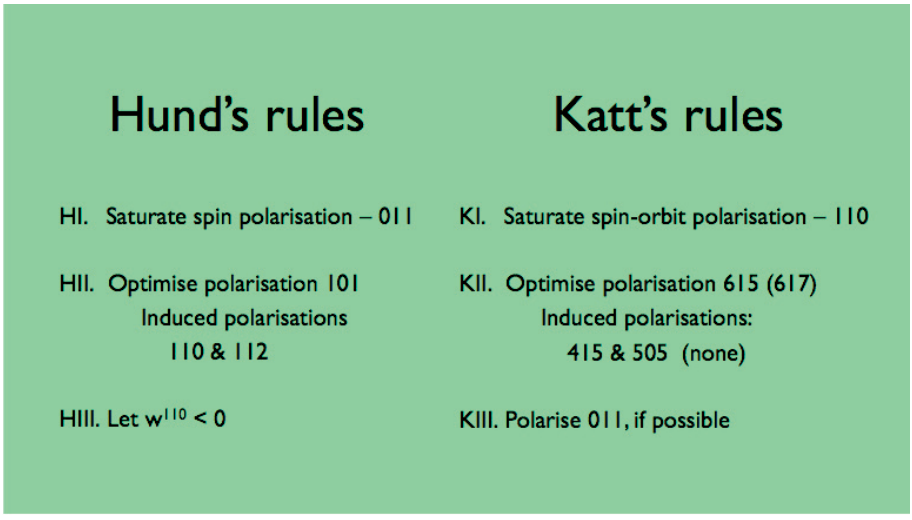

Figure 6.11: Formulation of Hund's and Katt's rules for a f-electrons system in the present formalism. For the KII rule the polarizations are given for an f-occupation of less (larger) than 6.

system will enhance the SOC in order to gain energy by polarizing the 110 channel; this is referred to as OP-even. The resulting state is still double degenerate due to TR symmetry. Secondly, this degeneracy can then efficiently be split by a polarization of the 615 channel (617 for more than half-filled f shell, as shown in Fig. 6.12). Since this is a rank-5 tensor, there are 11 independent components. In the case of tetragonal symmetry as in URu_2Si_2, there are only two independent components allowed; w_0^{615} and $w_4^{615} + w_{-4}^{615}$. It can be shown that the most optimal polarization in this case is a full polarization of the 0 component and a partial polarization of the ± 4 components. In addition small polarizations of 415 and 505 are requested in order to keep the density matrix physical. These polarizations of Katt's first and second rule are displayed in Fig. 6.13. In the calculations of magnetic uranium compounds we generally find a coexistence of polarizations of the 615 channel and the 011 channel. An analysis gives that a 011 polarization is always permitted, and usually favourable, whenever full saturation of the other channels have not been reached. However, most importantly, we obtain that when Katt's first and second rule are completely fulfilled, with a fully saturated $w_{\pm 4}^{615}$ tensor component, the SP is forbidden. Hence, these two types of polarizations are competing, in accordance with our results for URu_2Si_2 in Fig. 6.7. In this respect, the observation of a HO of URu_2Si_2 is the effect of the nearly optimal polarization of $w_{\pm 4}^{615}$ that prevents the usual SP.

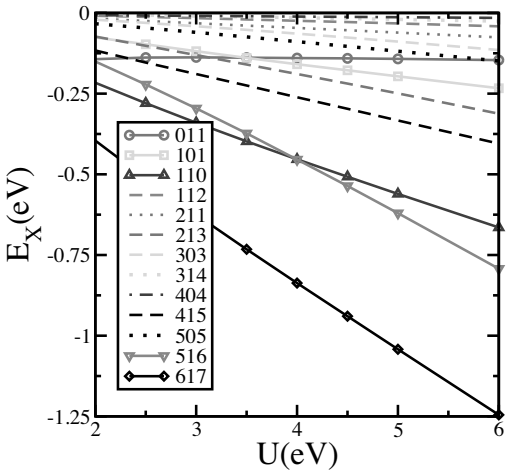

Figure 6.12: Exchange energy channels in ferromagnetic Cf in fcc structure, $a =$ 10.87 a.u., as unpolarized parameter U. The following channels are the most relevant: 617, associated with an high multipole of the magnetization, 516, related to an high multipole of spin-currents, and the SOC-like term 110.

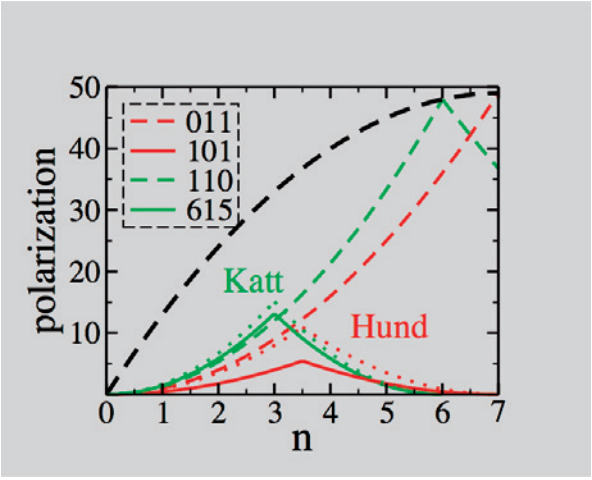

Figure 6.13: Comparison of Katt's and Hund's rule in terms of polarizations. The black line gives the maximum polarization. The red curves indicate the polarization according to Hund's rules: first the 011 polarization (dashed line) and then the 101 polarization (full line). The total polarization involved in the second rule, i.e. including the induced channels, is given by the dotted curve. The green curves give the polarizations according to Katt's rules; first the 110 polarization (dashed line) and then the 615 polarization (full line). The dotted line gives the total polarization involved in the second rule.

6.7 Low Spin Moment due to Hidden Multipole Order in ferro-pnictides

The discovery of a new family of materials with an high critical temperature (T_C) [13], the ferro-pnictides, has led to a resurgence of interest in superconductivity. In particular a hope was quickly raised that these compounds would finally lead to an understanding of the elusive mechanism of the superconductivity of the high-T_C cuprates. Indeed there are many common aspects; the fact that the parent compound is AF, the important role played by a transition-metal layer, the disappearance of the AF state with doping and the consequent transition to a superconducting state. However, some differences were also discovered, in particular the fact that the Fe d electrons in cuprates are correlated and close to an insulating state, while in the ferro-pnictides, they seem moderately correlated and metallic. This difference between the two types of materials is also underlined by the fact that first-principles calculations of the undoped ferro-pnictides obtain the correct AF order, while in the undoped cuprates they obtain a wrong non-magnetic metallic state. However, with the increasing number of theoretical studies, it has been clarified that DFT faces some difficulties in describing also the iron pnictide parent compounds. The calculations overestimates the ordered AF spin-moment, which is 0.35 μ_B in LaOFeAs [19]. For example GGA calculations overestimate the spin moment

by at least a factor 5, giving 2.0-2.5 μ_B [17, 18]. In this work we perform LDA+U calculations for the AF parent compound LaOFeAs. As described in paper I, the obtained results show that, for realistic U parameters, a low spin moment solution is stabilized due to polarization of higher multipole moments of the spin density. These terms can be analyzed as a spin orbital ordering among mainly the xz and yz d-orbitals at the Fe sites. It is also found that the calculated equilibrium distance between the Fe plane and the As planes is in good agreement with the experimental value [19]. Finally we make a comparison with the LDA+U solution for an undoped cuprate, $CaCuO_2$, which reveals a striking similarity in the role played by magnetic multipoles. The total energy as functionof the spin moment, as calculated by constraining the staggered spin moments [98] of the stripe ordered AF state, and as functionof U, is displayed in Fig. 6.14. In agreement with earlier studies [17] the GGA curve ($U = 0$) has a clear deep minimum at $m = 2.2\ \mu_B$. This minimum moves slightly to larger moments by increasing U. However, when the spin moment is constrained in the scan for other solutions, we can observe that a second solution starts to develop at a smaller moment. At $U \approx 2$ eV this has evolved to a local minimum, which becomes the global minimum for $U \gtrsim 2.5$ eV, a value close to the estimated one [99]. Hence there are several competing metastables states found, among which the low-moment solution is most stable in the case of LaOFeAs and for $U > 2$ eV. Both these magnetic solutions have an equilibrium Fe-As bonding distance in close agreement with experiments in contrast to the U=0 result, as shown in the inset of Fig. 6.14 for the case of U=2.75 eV. Hence, for physical values of U around 2.75 eV the calculations obtain a moment of 0.35 μ_B and $z_{As} = 0.650$, both in excellent agreement with experiment [19]. The exchange contribution to the total energy curve for U=2.5 eV of Fig. 6.14 is decomposed in the contributions from the multipoles $\boldsymbol{w}^{kp}$ according to Eq. (5.31). Besides the spin polarization energy, which is of course quadratic with the moment, there is a large exchange contribution from the magnetic multipole $\boldsymbol{w}^{41}$. Since this multipole has the largest magnitude for small moments where it dominates, it is the one that stabilizes the small and intermediate moment solutions for large enough U in Fig. 6.14. The most significant multipole tensor components $\boldsymbol{w}^{41}$ as functionof the constrained moment are also displayed in Fig. 6.15 in their tesseral form [72]. These large multipoles result in a very anisotropic magnetization density as seen in Fig. 6.16 for the case of U=2.75 eV, where the magnetization density has both large positive and negative values but integrates to a small value of 0.35 μ_B. Finally, we want to underline the fact that the multipole needed to stabilize the low moment solution, instead of the large moment solution as predicted by GGA, also plays a fundemental role in the formation of an insulating AF solution in the cuprates, as e.g. $CaCuO_2$. The multipoles and their energies for $CaCuO_2$ calculated with U=7.0 eV are shown in Fig. 6.15. In this case the existence of the multipole is easier to understand as it is essentially a pure $x^2 - y^2$ orbital that polarizes, giving arise to a non-spherical charge and mag-

netization density. However, the magnitude of the multipoles are of the same order as in LaOFeAs, and in fact, without these multipoles, the non-magnetic solution is more stable. This finding is in accordance with the fact that more exchange energy goes into the formation of the multipole than that of the spin moment. Hence, in both types of compounds it is the neglect of these multipole exchange channels in LDA and GGA that leads to the wrong ground state, with either too large (LaOFeAs) or too small moments ($CaCuO_2$). Then a crucial issue remains wide open; how do these spin and spin-orbital ordered AF ground states of the parent compound, with their significant formation energies, vanish already with a small doping, which eventually leads to a high T_C superconductivity? One can speculate that the multipole order in some form remains beyond the doping where the AF order is destroyed, and then constitutes the hidden order of the so-called pseudogap region, which is well established in the cuprates [100] and has been observed recently for the pnictides [101].

As presented in paper VI, after this first investigation, we performed a second study by evaluating the stability of different solutions corresponding to various arrangement of magnetic rank-4 multipoles for the most well-studied ferro-pnictides. For LaOFeAs, the lowest energy solution is then identified with a multipolar ordering of w^{41}_{-20} and w^{41}_{20} (tesseral form [72]) which, also in this case, gives raise to the correct value of experimental moment [19]. The same procedure is applied to $BaFe_2As_2$ and $CaFe_2As_2$ where the lowest energy solution correspond again to a combination of w^{41}_{20} and w^{41}_{-20} multipoles, but with a magnetic moment lower than the experimental value [102, 103]. However, for these compounds, our calculated moment constitutes a significant improvement over previous ab-initio calculations that largely overestimate the Fe moment [17, 104]. Moreover for $BaFe_2As_2$ and $CaFe_2As_2$, in the total energy curves as unpolarized constrained spin moment, we identify a local minima close to the experimental moment.

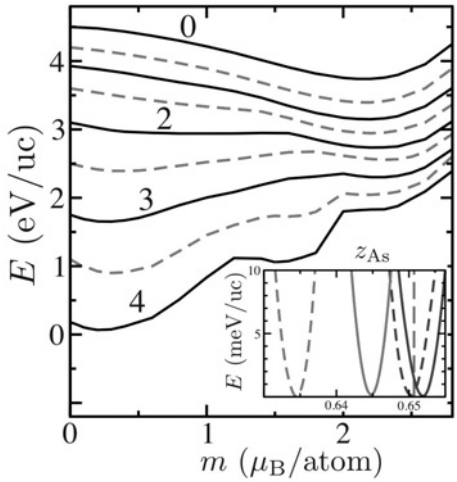

Figure 6.14: Total energy per magnetic unit cell (4 formula units) as functionof constrained staggered spin moment per Fe calculated with varying $0 \leq U \leq 4$ eV in steps of 0.5 eV (some values are indicated), with solid curves for integer values. The energy shifts between the curves are arbitrary and chosen in order to simplify the comparison. In the inset the energy is plotted as functionof z_{As} for U=0 (red) with minima at lower z_{As}, non-magnetic (dashed) and magnetic (full) solutions, and for U=2.75 eV (blue), low (dashed) and high spin (full) solutions. The experimental value [19] is indicated by a vertical line.

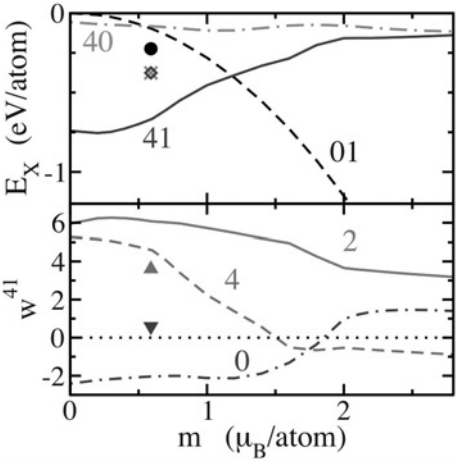

Figure 6.15: Exchange energy per Fe atom decomposed into multipole $\boldsymbol{w}^{kp}$ contributions (top, where the number indicates kp) and multipole tensor components w^{41}_{q0} (bottom, with numbers indicating q) as functionof the constrained spin moment per atom for a fixed U=2.5 eV. In addition the same quantities are shown with symbols obtained by a corresponding calculation for $CaCuO_2$ with U=7.0 eV and calculated m=0.59 μ_{B}.

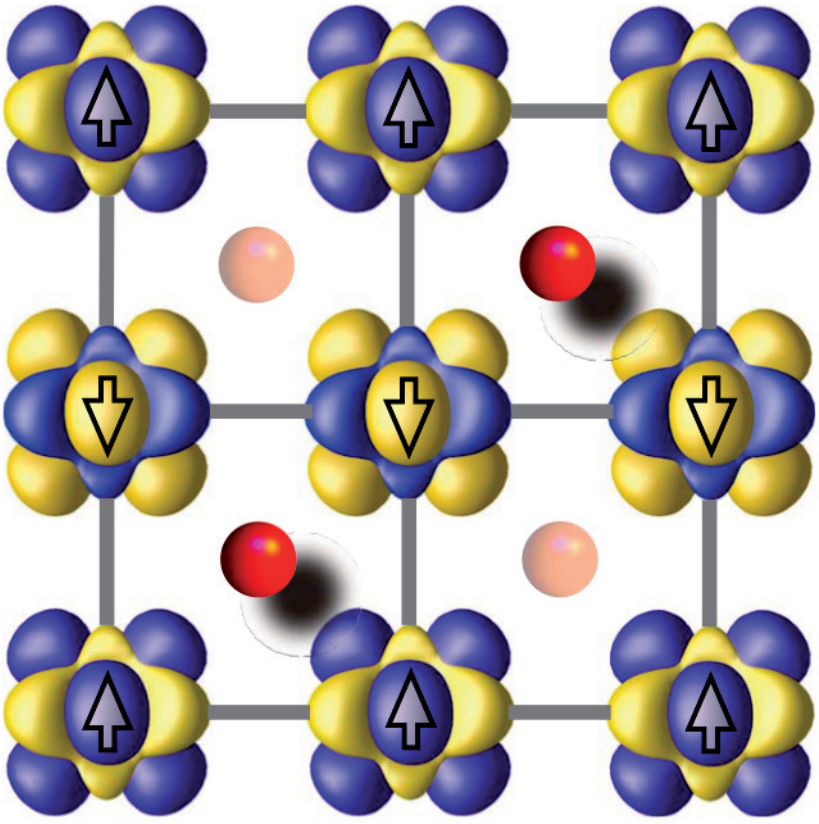

Figure 6.16: Isosurface plots of the magnetization density around the Fe sites for the striped AF order and U=2.75 eV are displayed with positive value indicated with dark/blue and negative with light/yellow. The arrows show the directions of the small integrated atomic dipole moments. The As atoms situated below and above the Fe-plane are displayed with spheres.

7. Conclusions

In this work we propose a convenient scheme to optimize the LDA+U procedure by reducing the number of free parameters to one. This is done by determining individually the Slater parameters through a screened Yukawa potential. In addition we argue to systematically use the interpolation approach [12] to double-counting (DC), which takes away the ever existing choice between AMF or FLL, especially since the results depend on the choice of DC. This approach ought to facilitate fast and systematic LDA+U calculations. The results of which would be comparable between different computations, without having to discuss on the used values of parameters. A combination of these two approaches has showed to be working very well in many actinide systems; it is able, for example to distinguish between magnetic and non-magnetic Pu compounds. Secondly, we present a method, the decomposition in tensor moments of the density matrix, that facilitates the analyzes of the results from an LDA+U study. This is an exact approach which gives both the different polarization channels as well as the corresponding Hartree and exchange energies. We apply these combined approaches to different actinide compounds in order to increase our understanding of the complicate behaviour of these systems, in particular the absence of magnetic moment in δ-Pu and the hidden order (HO) phase of the heavy-fermion superconductor URu_2Si_2. In case of δ-Pu we stabilize a non-magnetic solution in which the spin polarization (SP) channel 011 in the exchange energy is taken over by the orbital polarization (OP) even channel, 110. The magnitude of $\boldsymbol{w}^{110}$ is comparable to recent experiments for α-Pu [65]. In URu_2Si_2 we find that the non-trivial magnetic triakontadipole moments, associated with the tensor moments $\boldsymbol{w}^{615}$, constitute the HO parameter. We vary the in-plane lattice constant a to simulate the effect of pressure and we determine a critical value of a at which both spin and orbital moment disappear, while simultaneously the 615 contribution to the exchange energy almost diverges. The 615 channel is significant also in other uranium compounds, however what is unique in the case of URu_2Si_2 is that its polarization is so large that the usual dipole polarizations, e.g. SP, are forced to vanish. Our findings imply that there is always an HO in the magnetic actinides, but it is only when it forces the dipoles to vanish that it becomes perceptible. Moreover, the triakontadipole magnetic order is also found to play an essential roles in the hexagonal-based superconductors UPd_2Al_3, UNi_2Al_3 and UPt_3 and in the insulators dioxides UO_2, NpO_2 and PuO_2. In all actinide compounds we consider, except Cm, Hund's rules are far away from fulfilled,

since the SP does not play the dominant role as always assumed. We formulate an alternative set of rules, the Katt's rules, valid for itinerant systems in case of strong SOC interaction instead of those of Hund; one should first maximize the OP-even 110 channel, then saturate 615 channel, and only at the end try to maximize the SP 011, if still allowed.
Finally, we apply the method to the ferro-pnictides, a new class of high-T_C superconductors; in this case a low spin moment solution in agreement with experiment [19] is stabilized due to polarization of higher multipole moments of the spin density and parallels can be drawn to the stabilization of the antiferromagnetic order in cuprates, for example in $CaCuO_2$. One can speculate that the multipole order in some form remains beyond the doping where the antiferromagnetic order is destroyed, and then constitutes the HO of the so-called pseudogap region, which is well established in the cuprates [105] and has been observed recently for the ferro-pnictides [106].

Appendix

When Eq. (5.30) together with Eq. (5.18) are inserted in the exchange part of Eq. (5.1), we get an expression where the complications essentially arise from the orbital summations in the factor

$$\mathscr{Q} = \sum_{m_a m_b m_c m_d q} (-1)^q \begin{pmatrix} \ell & k_1 & \ell \\ -m_c & x_1 & m_a \end{pmatrix} \begin{pmatrix} \ell & k & \ell \\ -m_a & -q & m_d \end{pmatrix} \begin{pmatrix} \ell & k_2 & \ell \\ -m_d & x_2 & m_b \end{pmatrix} \begin{pmatrix} \ell & k & \ell \\ -m_b & q & m_c \end{pmatrix}, \tag{7.1}$$

where the indices on k and x stem from the two different density matrix expansions. The spin dependence of the exchange energy is simpler due to the Kronecker delta-symbols in Eq. (5.18), i.e. the relevant factor becomes

$$\begin{aligned} \mathscr{S} &= \sum_{s_a s_b s_c s_d} (-1)^{-s_c - s_d} \begin{pmatrix} s & p_1 & s \\ -s_c & y_1 & s_a \end{pmatrix} \delta_{s_a s_d} \begin{pmatrix} s & p_2 & s \\ -s_d & y_2 & s_b \end{pmatrix} \delta_{s_b s_c} \\ &= \sum_{s_a s_b} (-1)^{1+s_a-s_b} \begin{pmatrix} s & p_1 & s \\ -s_a & -y_1 & s_b \end{pmatrix} \begin{pmatrix} s & p_2 & s \\ -s_a & y_2 & s_b \end{pmatrix} = \\ &\quad (-1)^{1-y_1} [p_1]^{-1} \delta_{p_1 p_2} \delta_{y_1 - y_2} \end{aligned}, \tag{7.2}$$

by use of orthogonality relations. To simplify $\mathscr{Q}$ we start with an identity for the 6j-symbol, see e.g. Ref. [47], and we reshuffle a little,

$$\begin{Bmatrix} \ell & \ell & k_1 \\ \ell & \ell & k \end{Bmatrix} \begin{pmatrix} \ell & \ell & k_1 \\ m_b & -m_c & -x_1 \end{pmatrix} = \sum_{m_a m_d q} (-1)^{\ell+\ell+k+m_a+m_d+q} \times \begin{pmatrix} \ell & k & \ell \\ -m_d & -q & m_b \end{pmatrix} \begin{pmatrix} \ell & k & \ell \\ -m_c & q & m_a \end{pmatrix} \begin{pmatrix} \ell & k_1 & \ell \\ m_d & -x_1 & -m_a \end{pmatrix}. \tag{7.3}$$

Then we multiply by $\begin{pmatrix} \ell & \ell & k_2 \\ m_b & -m_c & x_2 \end{pmatrix}$ and sum over m_b and m_c, by obtaining

$$\begin{Bmatrix} \ell & \ell & k_1 \\ \ell & \ell & k \end{Bmatrix} \sum_{m_b m_c} \begin{pmatrix} \ell & \ell & k_1 \\ m_b & -m_c & -x_1 \end{pmatrix} \begin{pmatrix} \ell & \ell & k_2 \\ m_b & -m_c & x_2 \end{pmatrix}$$
$$= \sum_{m_a m_b m_c m_d q} (-1)^{k_1+k+x_1+q} \begin{pmatrix} \ell & k_1 & \ell \\ -m_d & x_1 & m_a \end{pmatrix} \begin{pmatrix} \ell & k & \ell \\ -m_a & -q & m_c \end{pmatrix}$$
$$\begin{pmatrix} \ell & k_2 & \ell \\ -m_c & x_2 & m_b \end{pmatrix} \begin{pmatrix} \ell & k & \ell \\ -m_b & q & m_d \end{pmatrix}. \tag{7.4}$$

On the LHS we use an orthogonality relation for the 3j-symbol and on the RHS we identify $\mathscr{Q}$ from Eq. (7.1)

$$\begin{Bmatrix} \ell & \ell & k_1 \\ \ell & \ell & k \end{Bmatrix} [k_1]^{-1} \delta_{k_1 k_2} \delta_{x_1 - x_2} = (-1)^{k_1+x_1+k} \mathscr{Q}. \tag{7.5}$$

The phase factors of Eqs. (7.2) and (7.5) are then used to form the scalar product of the double tensors in the final form of the exchange energy E_{X}, Eq. (5.42), as

$$\boldsymbol{w}^{k_1 p_1} \cdot \boldsymbol{w}^{k_1 p_1} = \sum_{x_1 y_1} (-1)^{x_1+y_1} w^{k_1 p_1}_{x_1 y_1} w^{k_1 p_1}_{-x_1 - y_1}. \tag{7.6}$$

8. Sammanfattning på svenska

Elektroner och kärnor är de grundläggande partiklar som bestämmer egenskaperna hos ett material. Grunden för förståelsen av materia vilar således på förståelsen av dess elektronstruktur. Paul Dirac skrev 1929 [1] i och med upptäckten av kvantmekaniken
"De grundläggande lagarna nödvändiga för den matematiska teorin som beskriver en stor del av fysiken samt all kemi är härmed helt kända. Svårigheten ligger nu i att applikationen av dessa lagar leder till ekvationer alltför komplicerade för att vara möjliga att lösa". Idag finns en effektiv metod där dessa ekvationer kan lösas med hjälp av superdatorer: densitetsfunktionalteori (DFT) [2]. I DFT omformuleras den explicita växelverkan mellan elektronerna så att varje elektron istället växelverkar med elektrondensiteten. Standard DFT har visat sig fungera utmärkt för många grupper av material, men misslyckas ofta med att beskriva system med öppna d och f skal, där elektronerna är lokaliserade och Coulomb repulsionen stark. För dessa materialen uppkommer problem med beskrivningen av elektronernas växelverkan som oberoende av varandra då en elektron beror på andra elektroners position; detta kallas att elektronerna är starkt korrelerade.

Trots att de magnetiska egenskaperna hos material har tillämpats i många år utgör forskningen kring magnetism ett viktigt fält inom materialvetenskap. Forskningen på detta område är mycket intensiv och fortfarande upptäcks revolutionerande effekter som beror på magnetiska interaktioner. Kampen mellan gitter, laddnig, spin och orbitala frihetsgrader leder till ett komplicerat jämviktstillstånd där ibland fascinerande fenomen uppstår. En grupp av material som påvisar rikligt med extraordinära magnetiska egenskaper är aktiniderna [3]. Här återfinns allt från itineranta magnetiska system till system som påvisar lokaliserad magnetism. I gränslandet mellan dessa extremer har vi material där elektronerna blir tunga, s.k. tunga fermioner. Detta ger en mängd avvikande fenomen, som t.ex. samexistens av supraledning och magnetism [4]. En av anledningarna till att så många exotiska magnetiska fenomen uppträder hos just aktiniderna är att vi har både stark spin-bankoppling (SBK) och stark utbytesväxelverkan mellan $5f$-elektronerna, som ger upphov till magnetismen. Teoretiska beräkningar där lokala densitets approximationen (LDA), eller den generaliserade gradient approximationen (GGA) används ger ofta bra grundtillståndsegenskaper

för metalliska system, men tenderar att underskatta det orbitalmoment som SBK ger upphov till [5, 6, 7]. Detta kan avhjälpas genom användning av t.ex. orbital polarization [7], som kommer av Hund's andra regel i atomfysik. Alternativt läggs en orbitalberoende potential till hamiltonianen, eller så används det så kallade LDA+U tillvägagångssättet [8, 9, 10]. Här används en skärmad Hartree-Fock (HF) interaktion endast för $5f$ elektronerna. Magnetism är vanligt bland aktiniderna, men vanligtvis är spinmomentet kraftigt reducerat i jämförelse med det fullt spinpolarizerade värdet.

Den här avhandlingen fokuserar på den roll de skärmade interaktionerna har och argumenterar för att de är orsaken till både det reducerade spinmomentet och det förstärkta orbitalmomentet i många aktinidföreningar. Ett av dom mest diskuterade fallen inom aktinidforskningen är avsaknaden av magnetiskt moment i den avvikande δ-fasen av Pu [3]. En förklaring till detta visas här vara att utbytesväxelverkan i SBKkanalen förstärks. I studien av tungfermionssupraledaren URu_2Si_2i en fas där ordningsparametern än så länge är dold för alla experiment [11] återfinns en högre ordningens multipol av magnetiseringsdensiteten, en triakontadipol, som den dominerande ordningsparametern. Triakondadipolen visar sig också spela en avgörande roll hos anda aktinidsupraledare, UPd_2Al_3, UNi_2Al_3 och UPt_3 och i isolatorerna UO_2, NpO_2 och PuO_2. Dessa resultat har lett fram till Katts regler, som ersätter Hunds regler för grundtillståndet hos itineranta system där SBK är stark. För att hantera dessa system har vi utvecklat ett effektivt tillvägagångssätt att behandla elektron korrelationen inom LDA+U metoden med endast en fri parameter. Det kan vi åstadkomma genom att använda slater parametrar skärmade med Yukawa potentialen samt genom att behnadla dubbelräkningen med en interpolationsmetod [12]. Den fria parametern kan vara t.ex. den lägsta Slater integralen U. Vi introducerar också en analysmetod för grundtillståndet i form av en exakt expansion av densitetsmatrisen och HF utbytesväxelverkan i termer av multipoler.

En annan grupp av material som har rönt enormt intresse är kupratsupraledare med hög kritisk temperatur (T_C), där ett märkligt samspel mellan supraledning och magnetism finns. Nyligen upptäcktes en ny grupp av hög-T_C supraledare baserade på järnpniktider [13]. Detta har ingett hopp om ökad förståelse även för hög-T_C kupraterna [14]. Likheterna mellan materialen är många: Grundföreningarna är båda antiferromagnetiska (AF), ett lager av övergångsmetall spelar en viktig roll i båda materialen samt att AF ordningen snabbt övergår till ett supraledande tillstånd då materialet dopas. Väsentliga skilldnader återfinns också: Kupraterna är isolatorer och elektronerna är starkt korrelerade, medans järnpniktiderna påvisar måttligt korrelerade elektroner och är metalliska [15, 16]. Av de många teoretiska studier som gjorts av järnpniktidsupraledarna är det uppenbart att DFT

har problem med beskrivningen, då en synnerligen dålig beskrivning av Fe-As bindningsavstånded erhålls, samt att AF spinmomentet överskattas grovt [17, 18]. Genom att tillämpa LDA+*U* metoden på järnpniktiderna erhålls en lösning med lågt spinmoment i enlighet med experiment [19]. Detta stabiliseras av högre multipoler av magnetiseringsdensiteten. Bindningsavståndet mellan Fe och As stämmer också det överens med experimentella värden [19]. Slutligen jämför vi med LDA+*U* lösningen av en odopad kuprat, $CaCuO_2$, som påvisar en mängd likheter i den roll som utspelas av dom magnetiska multipolerna.

Avhandligen är organiserad enligt följande: kapitel 2 går igenom densitetsfunktionalteorin för behandling av flerelektronsproblemet, kapitel 3 beskriver kraften hos APW+lo bassettet for att lösa Kohn-Sham ekvationerna, kapitel 4 summerar ickekollineär magnetism och kapitel 5 härleder LDA+*U* metoden och multipolexpansionen. Tillämpningen av dessa metoder på diverse aktinid- och pniktidföreningar diskuteras i kapitel 6, där vi observerar flera tydliga trender i vilken utbytesväxelverkanskanal som favoriseras. Slutligen summeras avhandlingen i kapitel 7.

Acknowledgements

First I would like to thank my supervisor Lars Nordström for teaching me everything I know about magnetism and material science and for the constant motivation. I wish to thank Kay Dewhurst and Sangeeta Sharma to have transmitted me their optimism by writing a DFT program (that works) from scratch. I must thank my second supervisor Peter Oppeneer for the precious discussions. I say thank you to my research team-mate and office-mate Oscar for all the help and discussions about science and life. I would like to thank Fredrik for having inspired me to start a Ph.d in this group by showing me his work on distorted plane-waves, for the fruitful collaboration over the past four years and for playing with his band at my dissertation party. I am grateful to Torbjörn for the endless enriching suggestions. Thank you Petros, Sebastien, Johan, Diana, Lars, big Andreas, Anders, Sergiu, Cecilia, Ralph, Moyses, Anden, Jan, Karel, Satadeep and Sumantha for believing my invented stories about Italy. I would like to thank the Italian crowd, Igor, Marco, Giuseppe, Andrea, Barbara and Fabrizio for disturbing me when I was working too hard. A special thank you to Biplab for the constructive science discussions and for the invitation to India. I am grateful to Jonas for having accompanied me for long walks in the crazy streets of Bombay. I am thankful to Patrik for arriving at work after me every morning (afternoon). I thank Martin for having picked up the only available double-room at the Jülich spring school, so that we did not have to stay for two weeks in a 16-people dorm room. I also thank Carlos to have succeeded to manage from Germany my accomodation needs in both Uppsala and Stockholm. I would like to thank Prof. Olle Eriksson and Prof. Börje Johansson for the good atmosphere they created in the group and Prof. Eberhard Gross for the kind hospitality in Berlin. I say thank you to Sasha Shick for the invitation to Prague. I am also grateful to Anatoly Belonoshko, for having shown me the secrets of molecular dynamics and for having inspired me to continue with a Ph.d in the field of condensed matter. I thank Peter for taking care of computers and Elizabeth for solving all bureaucracy issues. I also must wish a general thank you to all the members of our group for the stimulating research environment. Finally I would like to thank my brother Alessandro for coming to Sweden to teach me how to cook, and my parents for their constant support.

Bibliography

[1] P. DIRAC, *Proc. Roy. Soc.* **A 123**, 714 (1929).

[2] W. KOHN, *Rev. Mod. Phys.* **71**, 1253 (1999).

[3] K. T. MOORE and G. VAN DER LAAN, *Rev. Mod. Phys.* **81**, 235 (2009).

[4] G. R. STEWART, *Rev. Mod. Phys.* **56**, 755 (1984).

[5] T. KRAFT, P. M. OPPENEER, V. N. ANTONOV, and H. ESCHRIG, *Phys. Rev. B* **52**, 3561 (1995).

[6] P. M. OPPENEER, M. S. S. BROOKS, V. N. ANTONOV, T. KRAFT, and H. ESCHRIG, *Phys. Rev. B* **53**, R10437 (1996).

[7] M. S. S. BROOKS, *Physica B* **130B**, 6 (1985).

[8] V. I. ANISIMOV, I. V. SOLOVYEV, M. A. KOROTIN, M. T. CZYŻYK, and G. A. SAWATZKY, *Phys. Rev. B* **48**, 16929 (1993).

[9] A. I. LIECHTENSTEIN, V. I. ANISIMOV, and J. ZAANEN, *Phys. Rev. B* **52**, R5467 (1995).

[10] I. V. SOLOVYEV, A. I. LIECHTENSTEIN, and K. TERAKURA, *Phys. Rev. Lett.* **80**, 5758 (1998).

[11] M. B. WALKER, W. J. L. BUYERS, Z. TUN, W. QUE, A. A. MENOVSKY, and J. D. GARRETT, *Phys. Rev. Lett.* **71**, 2630 (1993).

[12] A. G. PETUKHOV, I. I. MAZIN, L. CHIONCEL, and A. I. LIECHTENSTEIN, *Phys. Rev. B* **67**, 153106 (2003).

[13] Y. KAMIHARA, T. WATANABE, M. HIRANO, and H. HOSONO, *Journal of the American Chemical Society* **130**, 3296 (2008).

[14] N. P. ARMITAGE, P. FOURNIER, and R. L. GREENE, *Rev. Mod. Phys.* **82**, 2421 (2010).

[15] M. NORMAN, *Physics* **1**, 21 (2008).

[16] Z. TESANOVIC, *Physics* **2**, 60 (2009).

[17] I. I. MAZIN, M. D. JOHANNES, L. BOERI, K. KOEPERNIK, and D. J. SINGH, *Phys. Rev. B* **78**, 085104 (2008).

[18] I. OPAHLE, H. C. KANDPAL, Y. ZHANG, C. GROS, and R. VALENTÍ, *Phys. Rev. B* **79**, 024509 (2009).

[19] C. DE LA CRUZ, Q. J. HUANG, J. W. LYNN, J. LI, W. RATCLIFF, J. L. ZARESTKY, H. A. MOOK, G. F. CHEN, J. L. LUO, N. L. WANG, and P. DAI, *Nature* **453**, 899 (2009).

[20] P. P. EWALD, *Ann. Phys.(Leipzig)* **54**, 519 (1917).

[21] P. HOHENBERG and W. KOHN, *Phys. Rev.* **136**, B864 (1964).

[22] M. LEVY, *Phys. Rev. A* **26**, 1200 (1982).

[23] N. W. ASHCROFT and N. D. MERMIN, *Solid state physics*, Brooks/Cole, 1976.

[24] E. WIGNER, *Phys. Rev.* **46**, 1002 (1934).

[25] D. M. CEPERLEY and B. J. ALDER, *Phys. Rev. Lett.* **45**, 566 (1980).

[26] P. D. ZIESCHE, S. KURTH, and P. PERDEW, *Comput. Mat. Science* **11**, 122 (1998).

[27] J. P. PERDEW, J. A. CHEVARY, S. H. VOSKO, K. A. JACKSON, M. P. PEDERSON, D. J. SINGH, and F. C., *Phys. Rev. B* **46**, 6671 (1992).

[28] D. SINGH and L. NORDSTRÖM, *Planewaves, Pseudopotentials and the LAPW Method, Second Edition*, Kluwer Academic Publishers Boston/Dordrecht/London, 2006.

[29] E. SJÖSTEDT and L. NORDSTRÖM, *Phys. Rev. B* **66**, 014447 (2002).

[30] E. SJÖSTEDT, L. NORDSTRÖM, and D. SINGH, *Solid State Commun.* **114**, 15 (2000).

[31] D. SINGH, *Phys. Rev. B* **43**, 6388 (1991).

[32] G. K. H. MADSEN, P. BLAHA, K. SCHWARZ, E. SJÖSTEDT, and L. NORDSTRÖM, *Phys. Rev. B* **64**, 195134 (2001).

[33] J. C. SLATER, *Phys. Rev.* **51**, 846 (1937).

[34] E. SJÖSTEDT and L. NORDSTRÖM, *J. Phys.: Condens. Matter* **14**, 12485 (2002).

[35] U. VON BARTH and L. HEDIN, *J. Phys. C* **5**, 1629 (1972).

[36] S. H. VOSKO, L. WILK, and M. NUSAIR, *Can. J. Phys.* **58**, 1200 (1980).

[37] W. KOHN and L. J. SHAM, *Phys. Rev.* **140**, A1133 (1965).

[38] C. HERRING, *Magnetism Vol. 4*, edited by G.T. Rado and H. Suhl, Academic Press, New York, 1963.

[39] L. M. SANDRATSKII and P. G. GULETSKII, *J. Phys. F: Met. Phys.* **16**, 43 (1986).

[40] Elk. An all-electron full-potential linearised augmented-plane wave plus local orbitals (FP-(L)APW+lo) code, available for free at http://elk.sourceforge.net.

[41] G. H. O. DAALDEROP, P. J. KELLY, and M. F. H. SCHUURMANS, *Phys. Rev. B* **41**, 11919 (1990).

[42] A. K. RAJAGOPAL and J. CALLAWAY, *Phys. Rev. B* **7**, 1912 (1973).

[43] E. U. CONDON and G. H. SHORTLEY, *The theory of atomic spectra*, University press, Cambridge, pp 174 of 1963 edition., 1935.

[44] A. B. SHICK, V. DRCHAL, and L. HAVELA, *Europhys. Lett.* **69**, 588 (2005).

[45] T. SHISHIDOU, T. OGUCHI, and T. JO, *Phys. Rev. B* **59**, 6813 (1999).

[46] M. R. NORMAN, *Phys. Rev. B* **52**, 1421 (1995).

[47] B. R. JUDD, *Operator Techniques in Atomic Spectroscopy*, McGraw-Hill, 1963.

[48] M. S. S. BROOKS, *J. Phys.: Condens. Matter* **22**, L469 (2001).

[49] I. V. SOLOVYEV, *Phys. Rev. Lett.* **95**, 267205 (2005).

[50] M. T. CZYŻYK and G. A. SAWATZKY, *Phys. Rev. B* **49**, 14211 (1994).

[51] J. ROSSAT-MIGNOD, G. LANDER, and P. BURLET, *Hand-book on the Physics and Chcmistry of the Actinidcs, Vol. 1*, eds. A.J. Freeman and G.H. Lander North-Holland, Amsterdam, 1984.

[52] J. C. SLATER, *Phys. Rev.* **34**, 1293 (1929).

[53] G. RACAH, *Phys. Rev.* **61**, 186 (1942).

[54] G. RACAH, *Phys. Rev.* **62**, 438 (1942).

[55] G. RACAH, *Phys. Rev.* **63**, 367 (1943).

[56] G. RACAH, *Phys. Rev.* **76**, 1352 (1949).

[57] G. VAN DER LAAN and B. T. THOOLE, *J. Phys.: Condens. Matter* **7**, 9947 (1995).

[58] G. VAN DER LAAN, *Phys. Rev. B* **57**, 112 (1998).

[59] S. Y. SAVRASOV and G. KOTLIAR, *Phys. Rev. Lett.* **84**, 3670 (2000).

[60] P. SÖDERLIND, *Europhys. Lett.* **55**, 525 (2001).

[61] J. C. LASHLEY, A. LAWSON, R. J. MCQUEENEY, and G. H. LANDER, *Phys. Rev. B* **72**, 054416 (2005).

[62] A. O. SHORIKOV, A. V. LUKOYANOV, M. A. KOROTIN, and V. I. ANISIMOV, *Phys. Rev. B* **72**, 024458 (2005).

[63] K. T. MOORE, G. VAN DER LAAN, M. A. WALL, A. J. SCHWARTZ, and R. G. HAIRE, *Phys. Rev. B* **76**, 073105 (2007).

[64] G. VAN DER LAAN, K. T. MOORE, J. G. TOBIN, B. W. CHUNG, M. A. WALL, and A. J. SCHWARTZ, *Phys. Rev. Lett.* **93**, 097401 (2004).

[65] G. VAN DER LAAN and B. T. THOLE, *Phys. Rev. B* **53**, 14458 (1996).

[66] K. T. MOORE, M. A. WALL, and R. G. HAIRE, *Phys. Rev. B* **78**, 033112 (2008).

[67] The elemental actinides are calculated with spin-polarized LDA and LDA+U method with INT type of double-counting. More specifically, U, $a^{\mathrm{U}} = 6.67$ a.u., and Np, $a^{\mathrm{Np}} = 6.65$ a.u., are calculated in their bcc phase with $U = 0.75$ eV and $U = 2.5$ eV, respectively. Pu, Am and Cm are calculated in their fcc phase with, respectively, $a^{\mathrm{Pu}} = 8.76$ a.u. and $U = 4$ eV, $a^{\mathrm{Am}} = 9.24$ a.u. and $U = 4$ eV, $a^{\mathrm{Cm}} = 9.52$ a.u. and $U = 5$ eV. The saturation value $\bar{w}^{110}$ is obtained as $\bar{w}^{110} = -\frac{4}{3}n_{5/2} + n_{7/2}$, where $n_{5/2}$ and $n_{7/2}$ indicate, respectively, the occupation of $j = 5/2$ and $j = 7/2$ states filled in an atomic manner, with the condition that $n_{5/2} + n_{7/2}$ is equal to the LDA+U $5f$-occupation.

[68] H. M. LEDBETTER and R. L. MOMENT, *Acta Metall.* **24**, 891 (1976).

[69] G. LANDER and P. BURLET, *Physica B* **215**, 7 (1995).

[70] M. BROOKS, *Physica B* **345**, 93 (2004).

[71] L. NORDSTRÖM and D. SINGH, *Phys. Rev. Lett.* **76**, 4420 (1996).

[72] A tesseral tensor x^r is related to the spherical tensor $\tilde{x}^r$ through $x^r_0 = \tilde{x}^r_0$ and $x^r_q = \left(\tilde{x}^r_{|q|} + (-)^q \tau \tilde{x}^r_{-|q|}\right)/\sqrt{2\tau}$ for $q \neq 0$, where $\tau = \mathrm{sgn}\, q$.

[73] T. T. M. PALSTRA, A. A. MENOVSKY, J. V. D. BERG, A. J. DIRKMAAT, P. H. KES, G. J. NIEUWENHUYS, and J. A. MYDOSH, *Phys. Rev. Lett.* **55**, 2727 (1985).

[74] M. B. MAPLE, J. W. CHEN, Y. DALICHAOUCH, T. KOHARA, C. ROSSEL, M. S. TORIKACHVILI, M. W. MCELFRESH, and J. D. THOMPSON, *Phys. Rev. Lett.* **56**, 185 (1986).

[75] Y. MIYAKO, S. KARAWAZARAKI, H. AMITSUKA, C. PAULSEN, and K. HASSELBACH, *J. Appl. Phys.* **70**, 5791 (1991).

[76] A. P. RAMIREZ, P. COLEMAN, P. CHANDRA, E. BRÜCK, A. A. MENOVSKY, Z. FISK, and E. BUCHER, *Phys. Rev. Lett.* **68**, 2680 (1992).

[77] T. T. M. PALSTRA, A. A. MENOVSKY, and J. A. MYDOSH, *Phys. Rev. B* **33**, 6527 (1986).

[78] A. DE VISSER, F. E. KAYZEL, A. A. MENOVSKY, J. J. M. FRANSE, J. VAN DEN BERG, and G. J. NIEUWENHUYS, *Phys. Rev. B* **34**, 8168 (1986).

[79] U. WALTER, C. LOONG, M. LOEWENHAUPT, and W. SCHLABITZ, *Phys. Rev. B* **33**, 7875 (1986).

[80] T. E. MASON and W. J. L. BUYERS, *Phys. Rev. B* **43**, 11471 (1991).

[81] C. BROHOLM, J. K. KJEMS, W. J. L. BUYERS, P. MATTHEWS, T. T. M. PALSTRA, A. A. MENOVSKY, and J. A. MYDOSH, *Phys. Rev. Lett.* **58**, 1467 (1987).

[82] P. SANTINI and G. AMORETTI, *Phys. Rev. Lett.* **73**, 1027 (1994).

[83] A. KISS and P. FAZEKAS, *Phys. Rev. B* **71**, 054415 (2005).

[84] V. BARZYKIN and L. P. GOR'KOV, *Phys. Rev. Lett.* **70**, 2479 (1993).

[85] P. CHANDRA, P. COLEMAN, J. MYDOSH, and V. TRIPATHI, *Nature* **417**, 831 (2002).

[86] C. M. VARMA and L. ZHU, *Physical Review Letters* **96**, 036405 (2006).

[87] S. ELGAZZAR, J. RUSZ, M. AMFT, and J. A. MYDOSH, *Nature Materials* **8**, 337 (2009).

[88] M. YOKOYAMA, H. AMITSUKA, K. TENYA, K. WATANABE, S. KAWARAZAKI, H. YOSHIZAWA, and J. A. MYDOSH, *Phys. Rev. B* **72**, 214419 (2005).

[89] A. KRIMMEL, P. FISHER, B. ROESSLI, H. MALETTA, C. GIEBEL, C. SCHANK, A. GRAUEL, A. LOIDL, and F. STEGLICH, *Z. Phys. B* **86**, 161 (1992).

[90] A. SCHRÖDER, J. G. LUSSIER, B. D. GAULIN, J. D. GARRETT, W. J. L. BUYERS, L. REBELSKY, and S. M. SHAPIRO, *Phys. Rev. Lett.* **72**, 136 (1994).

[91] G. AEPPLI, E. BUCHER, C. BROHOLM, J. K. KJEMS, J. BAUMANN, and J. HUFNAGL, *Phys. Rev. Lett.* **60**, 615 (1988).

[92] M. NORMAN, R. ALBERS, A. BORING, , and N. CHRISTENSEN, *Solid State Commun.* **68**, 245 (1988).

[93] G. MCMULLAN, P. ROURKE, M. NORMAN, A. HUXLEY, N. DOIRON-LEYRAUD, J. FLOUQUET, G. LONZARICH, A. MCCOLLAM, and S. JULIAN, *New J. Phys* **10**, 053029 (2008).

[94] E. HASSINGER, G. KNEBEL, T. MATSUDA, D. AOKI, V. TAUFOUR, and J. FLOUQUET, *preprint arXiv* **1010.1288** (2010).

[95] G. AMORETTI, A. BLAISE, R. CACIUFFO, J. M. FOURNIER, M. T. HUTCHINGS, R. OSBORN, and A. D. TAYLOR, *Phys. Rev. B* **40**, 1856 (1989).

[96] R. LASKOWSKI, G. K. H. MADSEN, P. BLAHA, and K. SCHWARZ, *Phys. Rev. B* **69**, 140408 (2004).

[97] P. SANTINI, S. CARRETTA, N. MAGNANI, G. AMORETTI, and R. CACIUFFO, *Phys. Rev. Lett.* **97**, 207203 (2006).

[98] P. H. DEDERICHS, S. BLÜGEL, R. ZELLER, and H. AKAI, *Phys. Rev. Lett.* **53**, 2512 (1984).

[99] M. AICHHORN, L. POUROVSKII, V. VILDOSOLA, M. FERRERO, O. PARCOLLET, T. MIYAKE, A. GEORGES, and S. BIERMANN, *Phys. Rev. B* **80**, 085101 (2009).

[100] T. TIMUSK and B. STATT, *Rep. Prog. Phys.* **62**, 61 (1999).

[101] T. KATO, Y. MIZUGUCHI, H. NAKAMURA, T. MACHIDA, H. SAKATA, and Y. TAKANO, *Phys. Rev. B* **80**, 180507 (2009).

[102] Q. HUANG, Y. QIU, W. BAO, M. A. GREEN, J. W. LYNN, Y. C. GASPAROVIC, T. WU, G. WU, and X. H. CHEN, *Phys. Rev. Lett.* **101**, 257003 (2008).

[103] A. I. GOLDMAN, D. N. ARGYRIOU, B. OULADDIAF, T. CHATTERJI, A. KREYSSIG, S. NANDI, N. NI, S. L. BUD'KO, P. C. CANFIELD, and R. J. MCQUEENEY, *Phys. Rev. B* **78**, 100506 (2008).

[104] D. J. SINGH, *Phys. Rev. B* **78**, 094511 (2008).

[105] T. TIMUSK and B. STATT, *Rep. Prog. Phys.* **62**, 61 (1999).

[106] T. KATO, Y. MIZUGUCHI, H. NAKAMURA, T. MACHIDA, H. SAKATA, and Y. TAKANO, *Phys. Rev. B* **80**, 180507 (2009).

[107] U. FANO, *Rev. Mod. Phys.* **29**, 74 (1957).

[108] H. AMITSUKA, M. SATO, N. METOKI, M. YOKOYAMA, K. KUWAHARA, T. SAKAKIBARA, H. MORIMOTO, S. KAWARAZAKI, Y. MIYAKO, and J. A. MYDOSH, *Phys. Rev. Lett.* **83**, 5114 (1999).

Acta Universitatis Upsaliensis

Digital Comprehensive Summaries of Uppsala Dissertations from the Faculty of Science and Technology 775

Editor: The Dean of the Faculty of Science and Technology

A doctoral dissertation from the Faculty of Science and Technology, Uppsala University, is usually a summary of a number of papers. A few copies of the complete dissertation are kept at major Swedish research libraries, while the summary alone is distributed internationally through the series Digital Comprehensive Summaries of Uppsala Dissertations from the Faculty of Science and Technology. (Prior to January, 2005, the series was published under the title "Comprehensive Summaries of Uppsala Dissertations from the Faculty of Science and Technology".)

Distribution: publications.uu.se
urn:nbn:se:uu:diva-132068

ACTA
UNIVERSITATIS
UPSALIENSIS
UPPSALA
2010